CHALMERS

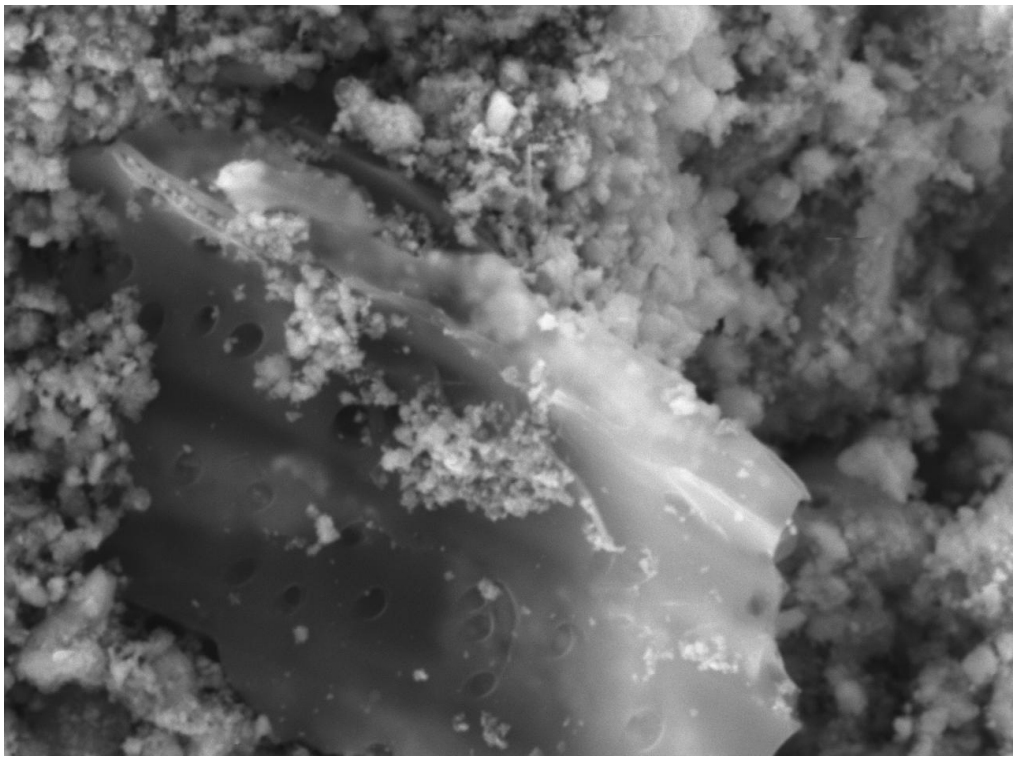

Production of Activated Biochar from Acacia Wood for Carbon Dioxide Capturing

Effects of Different Red Mud ratios as Mineral Activation Agents and Comparison with NaOH

Bachelor's Thesis in Chemical Engineering

Noah Friström
Anna-Alexandra Kim

Department of Chemistry and Chemical Engineering

CHALMERS UNIVERSITY OF TECHNOLOGY
Göteborg, Sweden 2026
www.chalmers.se

BACHELOR'S THESIS 2026

Production of Activated Biochar from Acacia Wood for carbon dioxide capturing

Effects of Different Red Mud Ratios as Mineral Activation Agents and Comparison with NaOH

Noah Friström
Anna-Alexandra Kim

Department of Chemistry and Chemical Engineering
Chalmers University of Technology
Ha Noi University of Science & Technology
Gothenburg, Sweden 2026
Ha Noi, Vietnam 2026

Supervisor: GS.TS. Lê Minh Thắng, Department of Chemistry and Chemical Engineering & Tạ Đình Quang, Department of Chemistry and Chemical Engineering
Examiner: Gunnar Westman, Professor, Department of Chemistry and Chemical Engineering

Bachelor's Thesis 2026
Department of Chemistry and Chemical Engineering
Ha Noi University of Science & Technology
Chalmers University of Technology

Abstract

The increasing concentration of carbon dioxide (CO_2) in the atmosphere has created a growing need to find efficient and sustainable carbon capture technologies. This study investigates the production of activated biochar from acacia wood using different ratios of red mud as a mineral based activation agent, with NaOH activation included for comparison.

Biochar was produced through pyrolysis following impregnation with different biomass to activation agent ratios (1:1 and 1:3 for red mud, and 1:3 for NaOH). The materials were characterized using SEM–EDX and BET surface area analysis, and their CO_2 adsorption performance was evaluated using gas chromatography.

The results showed that increasing the red mud ratio from 1:1 to 1:3 led to higher mineral content and reduced carbon content, accompanied by a decrease in specific surface area from 94 m^2/g to 74 m^2/g. This indicates that higher red mud loading may hinder pore development. In contrast, NaOH activation resulted in a significantly higher surface area (313 m^2/g), confirming its effectiveness in producing porous carbon structures.

Despite the lower surface area, red mud–activated biochar exhibited comparable or slightly higher CO_2 adsorption capacity, although with limited regeneration performance. Gas phase analysis revealed higher carbon monoxide formation for red mud samples, highlighting potential environmental risks.

Overall, red mud shows potential as a sustainable activation agent, but its performance is strongly dependent on activation ratio and remains limited compared to conventional NaOH activation.

Acknowledgements

We would first and foremost like to express our sincere gratitude to our examiner Dr. Prof. Le Minh Thang, for the opportunity to conduct this study at the Catalyst Laboratory in Vietnam. This experience would not have been possible without her support, and we are deeply grateful. She has been not only an inspiration within the research community but also a personal role model. Her guidance, ideas and encouragement have contributed significantly to our development as students, laboratory practitioners and team members.

We would also like to thank our supervisor and laboratory manager, Mr. Quang, for his continuous support, guidance, and for patiently answering our many questions throughout our time in Vietnam. Without his constant presence and assistance, this work would not have been possible. We are also grateful for introducing us to the Vietnamese culture and cuisine, which greatly enriched our overall experience.

A special thank you is also extended to the members of the GeViCata Laboratory for not only guiding us through our work but also for their warm welcome and for making us feel at home during our stay.

We would further like to thank our examinator at Chalmers University of Technology, Gunnar Westman, for ensuring we stayed on track and guiding us throughout the process of writing this bachelor thesis. We also greatly appreciate his continuous support, not only in our academic work but also through his genuine care for our well being during our stay.

Finally, we would like to acknowledge Minor Field Studies (MFS) and SIDA for funding our stay and travel expenses in Vietnam. Without this scholarship, this thesis would not have been possible. This opportunity not only allowed us to conduct research abroad but also contributed significantly to our personal and academic development. Living and working in a foreign country broadened our cultural awareness, our social skills and provided a truly valuable experience, for which we are very grateful.

Table of Contents

1 Introduction

The increasing levels of greenhouse gases in the atmosphere are among the most urgent challenges facing society today, especially carbon dioxide (CO_2) emissions. These emissions contribute to global warming, climate change, and ocean acidification [1], creating a pressing need for effective carbon capture technologies. Among various approaches, adsorption using porous carbon, activated carbon, and biochar materials has become a promising and energy efficient method for CO_2 capturing [2].

Activated carbon can be produced from biomass via pyrolysis followed by activation. This results in the production of porous structures with high specific surface areas that are suitable for gas adsorption. However, the performance of these materials strongly depends on factors such as the choice of activation agent, process conditions, and the properties of the precursor biomass [3].

Conventional chemical activation agents, such as NaOH and KOH, are highly effective in generating well developed pore structures [4]. However, these methods rely on synthetic chemicals and often involve environmentally problematic processing steps, including the generation of alkaline waste streams [5]. Therefore, there is an increasing interest in exploring alternative activation strategies based on waste derived materials.

One waste derived material is red mud, a by-product from the Bayer process in alumina production. Red mud is produced in large quantities worldwide and is often considered a waste disposal problem [6]. However, due to its high content of metal oxides, it is expected to contribute to increase surface area of the obtained carbon adsorbent. Moreover, its content of sodium has been shown to exhibit catalytic properties that may also promote pore development during pyrolysis [7]. Utilizing red mud as an activation agent presents an opportunity to convert two waste streams, biomass and industrial residue, into a functional material for CO_2 capture.

In addition to structural properties, the surface chemistry of activated carbon plays an important role in CO_2 adsorption. Introducing nitrogen containing functional groups can enhance adsorption performance by creating additional acid base interactions between the adsorbent and CO_2 molecules [7]. Nitrogen modification can therefore provide a complementary strategy to improve adsorption capacity beyond physical adsorption alone.

This thesis investigates how the biomass to red mud ratio influences the structural and compositional properties of biochar and its performance for CO_2 adsorption. The study further evaluates this waste-based activation strategy by comparing it with conventional NaOH activation. Additionally, the effect of nitrogen modification on selected biochar samples is examined to assess its potential for improving CO_2 adsorption performance.

2 Theory

This chapter covers all the necessary theory about how activated carbon can be utilized for CO_2 adsorption. It explains how activated carbon is produced from biomass using activation agents, as well as the role of pyrolysis conditions in converting biomass into porous materials such as biochar and activated carbon. In addition, it describes how activated carbon can be modified through aqueous nitrogen doping. Finally, a brief overview of the analytical methods applied in this project is provided.

2.1 Biomass as a Precursor for Activated Carbon

Biomass is composed of residues from plant-based materials and is referred to as lignocellulosic biomass. These materials contain a high proportion of carbohydrates, meaning they have a high carbon content [8]. This makes the material a promising precursor for producing active carbon through biochar. However, the yield of the biochar during pyrolysis depends strongly on the composition of the biomass [3].

Lignocellulosic biomass consists of three main organic polymers often referred to as pseudo-components: cellulose, hemicellulose, and lignin [3]. These components decompose at different temperatures due to their distinct chemical structures. Hemicellulose primarily decomposes at lower temperatures, usually around 220-315 °C, due to its branched architecture [9]. The weak bonding of the side chains causes them to break easily by thermal cracking during the pyrolysis process. As a result of their thermal instability, hemicellulose degrades into volatile organic compounds such as gases and a small amount of bio-oil. Cellulose is a linear polymer that is held together by strong intramolecular hydrogen bonds. These bonds make the thermal stability of the molecule significantly higher than that of hemicelluloses. Thus, it causes the molecule to possess a stable crystalline structure [3, 10]. Cellulose starts decomposing in the range of 300-400 °C, forming volatile compounds like mainly bio-oil and a little gas [9]. In contrast, lignin has a more thermally stable aromatic structure, which promotes the formation of solid carbon residue. As a result, lignin contributes to most biochar formation and therefore strongly influences the biochar yield [10]. Lignin decomposes at 150-900 °C [9].

Due to these differences in thermal stability and their decomposition processes, the relative proportions of cellulose, hemicellulose, and lignin in a biomass strongly influence the yield of the biochar. Biomasses with higher lignin content generally produce higher yields due to the aromatic and thermally stable structure.

In this study, acacia wood was selected as the biomass precursor. Acacia wood is a hardwood species that typically contains approximately 20-30% lignin. The high lignin content promotes the formation of solid carbon during pyrolysis, making acacia wood a suitable precursor for the production of activated carbon [11].

2.2 Chemical Activation before Pyrolysis

The use of activation agents prior to pyrolysis is a well-known strategy to enhance the development of porous carbon materials [12, 13]. Impregnation of the biomass before thermal decomposition allows the activating agent to interact with the biomass structure, functional groups, and cell wall matrices [14, 15]. During pyrolysis, biomass undergoes thermal decomposition, producing biochar, condensable liquids, and gaseous products [12]. Without prior impregnation, the resulting biochar often exhibits low specific surface area and limited pore development [16].

Using an activation agent influences thermal decomposition by promoting dehydration, decarboxylation, depolymerization reactions, and gas evolution [15]. These reactions in turn promote the formation of pores within the carbon matrix, which enhances the specific surface area (SSA) [12, 15].

Activation agents may also alter the surface chemistry of the biomass by interacting with oxygen-containing functional groups [17]. These interactions can affect carbon framework stability and adsorption properties [14, 15].

However, the amount of activation agents must be carefully controlled. Insufficient amounts of agent may lead to biochar not reaching its full potential with an underdeveloped pore structure. In contrast, too much activation can cause overconsumption of carbon, structural degradation, and pore collapse/blocking [2]. Therefore, optimization of the ratio of the activation agent is critical for achieving a balance between the positive and negative effects.

2.2.1 Red Mud

Red mud is a by-product from the Bayer process of production of alumina from bauxite ore [6]. The red mud used in this study comes from the Tan Rai Manufactory (Lam Dong Aluminium-Bauxite Complex Project), Lam Dong Province, Vietnam. The chemical composition of red mud depends on which plant it comes from. The general composition of red mud is metal oxides and residual alkaline compounds such as NaOH and KOH, and it exhibits catalytic properties that can be utilized as a mineral-based activation agent [2]. Red mud is currently a largely underutilized resource and is commonly regarded as an industrial waste product. This makes it an interesting candidate for exploring new application areas and further optimizing its performance as an activation agent. Utilizing red mud for this purpose enables the conversion of two waste materials, biomass and red mud, into a more sustainable solution for CO_2 capture. Such an approach would provide a valuable application for red mud, which is produced in large quantities worldwide.

In more detail, the red mud consists of metal oxides such as SiO_2, Al_2O_3, and an abundance of Fe_2O_3 [6]. The exact composition varies due to the original composition of the bauxite ore. Specifically for our case, we used locally produced red mud from Vietnam, which was studied and characterized using SEM–EDX analysis, confirming the presence of Fe, O, Al, Si, and Na. This composition generally gives the activation agents properties like high alkalinity and a pH of 12. The different metal oxides contribute to different catalytic reactions, where Fe_2O_3 is the most favourable [18].

During thermal treatment of a biomass, primed with red mud, Fe_2O_3 has been shown to act as an oxygen carrier which promotes cleavage of biopolymers [19]. It also enhances the dehydration and decarboxylation reactions due to Fe_2O_3 ability during anaerobic conditions, providing catalytically active sites in the form of metal ions [20]. The Fe_2O_3 has been proposed to form an unstable intermediate with -COOH, forming -COOFe, which reduces the binding energy. This increases gas evolution, lowers the tar production, and simultaneously promotes the carbon yield [18].

As a direct result of using red mud as an activation agent during pyrolysis of biomass, it allows lower temperatures for effective carbonization, yielding a better conversion rate of biomass to biochar and enhancing a better surface area because of the promotion of gas evolution [18, 6, 21, 22, 19]. However, excessive use of any activation agent may lead to problems such as pore blocking or pore collapse [18].

2.2.2 NaOH

Using NaOH as an activation agent is already a conventional method and is widely used in the production of activated carbon [4]. NaOH participates directly in chemical reactions with carbon during thermal treatment [5].

During thermal treatment, NaOH reacts with the carbon and oxygen functional groups, leading to carbon etching and structural rearrangement. This promotes the formation of gaseous production, which in turn leads to greater pore development [5].

At higher temperatures during pyrolysis, NaOH may also form intermediate sodium compounds such as Na_2CO_3 or Na_2O, which further contribute to pore formation through chemical reactions with carbon [23].

While NaOH is an effective way of producing pore-rich biochar, it relies on synthetic chemicals and produces other waste streams, such as alkaline wastewater during washing of the biochar [5]. For this reason, alternative activation agents such as red mud are of interest as a potentially more sustainable option. Based on previous studies and in the GeViCat laboratory, a biomass:NaOH ratio of 1:3 was the only ratio selected for comparison, as this ratio previously produced the highest specific surface area for similar biomass materials [24].

2.3 Pyrolysis of biomass

During pyrolysis of biomass, the components of biomass are decomposed in an oxygen-deprived environment through a gradual increase in temperature [25]. As described in “Biomass as a precursor for activated carbon”, the main components of biomass are hemicellulose, cellulose, and lignin [26]. This results in the production of biochar, a carbon-rich solid material.

The first components to decompose are hemicellulose and cellulose at the temperature range of 200-400 °C. Functional groups such as -OH and -COOH are eliminated, producing gaseous products such as CO_2, CH_4, CO, H_2O, and H_2 [26, 27]. The release of these gases promotes the porous attributes when they leave the solid structure, creating voids in the carbon matrix [25]. As the temperature

rises, lignin starts to decompose, and the aromatization of the carbon begins to occur. This makes the carbon more ordered, resulting in a more thermally stable material [26, 27].

Pyrolysis of biomass mainly produces three products in three different phases: A gaseous phase, a liquid phase, and a solid phase. The gas phase consists of non-condensable gases like H_2, CO, CO_2, and CH_4. The liquid phase is often referred to as tar and consists of bio-oil containing complex oxygenated compounds. The solid phase is the biochar, which serves as our precursor to the activated carbon [28].

Previous studies have shown that the distribution of the three product streams is highly influenced by the temperature [29]. Where a lower temperature leads to higher amounts of the solid phase, and a higher temperature promotes a bigger gaseous phase. This is because at higher temperatures, secondary cracking accelerates, resulting in increased formation of gases [30].

2.4 Acetone & Water Washing of the Biochar

During pyrolysis of biomass, various condensable organic compounds such as tar can be formed. These compounds may stick to the surface of the produced biochar or inside the pore structure, potentially blocking and limiting surface area [31]. In addition, other organic compounds such as polycyclic aromatic hydrocarbons (PAHs) and dioxin-like compounds may be produced during pyrolysis [32].

Previous studies have shown that washing treatments can remove these compounds from the biochar. Washing with water can remove soluble organic residues and reduce the presence of unwanted compounds, in turn improving surface area [32].

In this study, acetone was first used as an organic solvent to dissolve and remove tar-like organic residues that may remain on the biochar. Acetone is commonly used as an extraction solvent of organic compounds due to its ability to dissolve a wide range of nonpolar and moderately polar substances [33].

2.5 Modification of activated carbon with nitrogen

A common method to improve the adsorption of CO_2 is to modify the activated carbon with additional nitrogen functional groups [7, 38, 41]. Unmodified activated carbon captures the CO_2 through physical interactions [36, 40, 42]. Adding nitrogen in the structure of the activated carbon adds an additional way of capturing the CO_2, by acid-base interactions [35, 38, 39].

Replacing the acidic groups on the activated carbon with basic groups like nitrogen functionalities will promote CO_2 adsorption since the CO_2 by nature is slightly acidic [7, 35, 38]. It will also help enhance the selectivity of the adsorption [39, 42]. Creating basic-acid interactions to complement the Van der Waals forces between the walls and CO_2 [35, 40].

Introducing nitrogen to the activated carbon can be done in different ways. Either through gas-phase ammonia, impregnation with amine polymers, or aqueous hydrothermal treatment [7, 38, 41]. This report will focus on the latter.

Nitrogen in the form of aqueous ammonia is introduced to the activated carbon through hydrothermal treatment in an autoclave. Elevated temperature and pressure allow the nitrogen to bind to the carbon surface [34, 37, 39]. This is a method that allows nitrogen functionalization while still protecting the porous structure of the activated carbon [34, 39].

The modification of the activated carbon retains the reversibility but affects how CO_2 coordinates to the surface. [38, 42]. The regeneration of the activated carbon is done in the same way as unmodified carbons since the acid-base bonds are stronger than the Van der Waals bonds, but still reversible. It can be done by changing the temperature and/or pressure [36, 38, 42].

2.6 Using activated carbon to capture CO_2

Activated carbon (AC) is a material consisting primarily of carbon, with typically around 85% to 95% of its content being carbon. The remaining percentage is composed of heteroatoms such as oxygen, hydrogen, or nitrogen [43]. Activated carbon can be produced by a wide range of carbon-containing materials, such as wood, agricultural waste, and coal. Preferably, the precursor has a high carbon content [43, 44].

Using activated carbon for gas adsorption is favoured because of its unique porous nature, which in turn benefits to the activated carbon's large specific surface area. Carbon dioxide is a small molecule with a kinetic diameter of 0.33nm [46]. This allows the small molecule to enter the activated carbon's pores. Once inside the pores, the CO_2 hits the walls of the AC, resulting in a physical adsorption governed by weak intermolecular Van der Waals bonds to the carbon surface [43-45].

Previous studies have shown that the size of the pores is a primary factor of the CO_2 adsorption performance [44]. Micropores (<2nm) [45] enable more possible Van der Waals bonds between the pore walls of the AC and the CO_2. However, the appropriate effective size of the pores is also affected by the temperature and pressure conditions under which the adsorption takes place [44].

An important factor of the AC is its ability to regenerate through desorption of the adsorbed CO_2. This could be achieved by changing the temperature or the pressure. By sufficiently changing the

conditions, the weak Van der Waals bonds break and release the CO_2 again, making it possible to reuse the AC to capture new CO_2 [43, 44].

2.7 Analytic methods to determine the quality of AC

In this section, the analytical methods used to evaluate the quality of the activated carbon are introduced. The performance of the material is assessed through its surface morphology, elemental composition, specific surface area, and CO_2 adsorption behavior. Scanning Electron Microscopy combined with Energy Dispersive X-ray Spectroscopy (SEM–EDX) is used to investigate the surface structure and elemental distribution. The Brunauer–Emmett–Teller (BET) method is applied to determine the specific surface area and porosity of the materials. Additionally, CO_2 adsorption and desorption measurements are used to evaluate the adsorption capacity and regeneration performance of the produced biochar.

2.7.1 Scanning Electron Microscopy & Energy Dispersive X-ray Spectroscopy (SEM-EDX)

Scanning Electron Microscopy is an analytical method used to investigate the surface morphology and structural features of solid materials. During SEM, a focused beam of high-energy electrons scans across the sample surface, which makes the studied material emit secondary electrons that are detected to produce high-resolution images of the surface topography [48].

It's a particularly useful analysis method to study porous carbon materials, since it provides a high-resolution image, and information about the particle morphology, surface texture, and larger pore structures can be inspected. However, micropores, which are the primary CO_2 adsorbers, cannot be visualized with this method [48, 49].

Energy Dispersive X-ray Spectroscopy, coupled to the SEM instrument, was used to analyse the elemental composition of different materials. When the electron beam ejects inner-shell electrons from atoms in the sample, outer-shell electrons fill vacancies and emit element-specific X-rays. The X-rays can be detected, allowing identification of semi-quantitative estimation of elemental composition [48].

2.7.2 BET (Brunauer–Emmett–Teller) Method

Brunauer-Emmett-Teller method relies on physisorption to determine the specific surface area of a porous material. The physisorption method implies that the adsorption of the inert gas can be reversed due to no chemical bonds being formed. During the adsorption of an inert gas, the only forces being formed and broken are the van der Waals bonds that bind to the surface of the solid mass [50]. However, the interaction between the surface and other gases in the air occurs constantly without them bonding. Consequently, to maximize the amount of nitrogen gas absorbed onto the activated carbon, the interaction must take place in a controlled environment at low temperatures or in isothermal conditions. While the temperature is constant, the gas concentration and the pressure increase.

2.7.3 CO_2 Adsorption & Regeneration

The performance of a CO_2 adsorbent, such as activated carbon, can be evaluated based on its capacity to both capture and release CO_2. Gas chromatography (GC) is commonly used to quantify CO_2 concentrations during adsorption and desorption experiments [47]. By measuring the concentration of CO_2 in the gas phase before and after interaction with the adsorbent, it is possible to determine the net amount of CO_2 adsorbed.

During regeneration, the adsorbent is reheated, causing the adsorbed CO_2 to be released. By analysing the gas phase during this step using GC, the amount of desorbed CO_2 can be quantified. Together, the adsorption and desorption data provide a comprehensive evaluation of the performance of the carbon-based adsorbents, including both their adsorption capacity and regeneration behaviour.

3 Materials and Methods

This chapter describes the material and methods used in this study. It briefly outlines the materials and chemicals used, as well as their sources. The procedures for the biochar production are described in terms of ratios rather than exact quantities. Finally, the analytical methods used to characterize the materials produced are presented, including the operation conditions of the instruments.

3.1 Raw Materials

Acacia wood was used as the biomass precursor for biochar production. The material was obtained locally in Vietnam.
Red mud, a by-product from the Bayer process of alumina production, was used as a mineral-based activation agent. The red mud was sourced locally in Vietnam.
Sodium hydroxide (NaOH, analytical grade, ≥98% purity) was used as a chemical activation agent for comparison experiments.
Nitrogen gas (≥99.99% purity) was used to provide an inert atmosphere during pyrolysis.
Carbon dioxide gas (≥99.99% purity) was used in adsorption measurements.
Acetone and distilled water were used for washing and filtration procedures.
Liquid nitrogen was used in the BET procedure to ensure very low temperatures to halt any possible chemical reactions.
NH_3 solution 25% (Xilong, China) was used to nitrogen-modify the biochar.

3.2 Preparation of Activated Biochar

Acacia wood and red mud were sieved separately through mesh sieves to obtain uniformly sized particles in the range of 0.40mm to 0.20mm. The materials were then placed in separate beakers and dried in an oven at 100 °C for 4h to remove any moisture.

Two different suspensions were prepared with different mass ratios of biomass:redmud:water; 1:1:1, respectively 1:3:3. The suspensions were thoroughly mixed to ensure homogenous distribution before allowing them to impregnate for 5 days at room temperature.

For comparison, biomass was also impregnated using NaOH as an activation agent. A mass biomass:NaOH:water ratio of 1:3:3 was prepared. The dry biomass was first mixed with solid NaOH, after which the mixture was slowly added to water under continuous stirring. When homogeneous, it was left to impregnate for 5 days at room temperature.

Ceramic boats were filled with the wet mixtures. It was placed in the centre of the horizontal furnace (Lenton Thermal, Hope Valley, United Kingdom). A gas-phase collection system is constructed together with a nitrogen purge system.

After the isolation of the furnace system was completed, the furnace was purged of oxygen by pumping N_2 through the system at 60mL/min for 15 min. The nitrogen flow was then stopped, and the furnace was heated up at a rate of 20 °C/min.

When the temperature reached 400 °C, the nitrogen flow was resumed to ensure no oxygen was present inside the furnace. The nitrogen flow was maintained for 30 minutes. Simultaneously, the first gas-phase bag was filled from 400-450 °C. The bag was replaced with a new bag during the temperature range of 500-550 °C. Lastly, one last bag was filled with outlet gases at 550 °C.

After 30 minutes of nitrogen flowing, the valve was closed, and the pyrolysis was held at 550 °C for 1h. After 1h, the heating was turned off, letting the furnace cool down overnight with the samples still inside the oven.

The newly produced biochar was removed from the ceramic boats and weighed. It was placed in a beaker together with a 2.5x more acetone than biochar by weight, in order to remove any residual organic compounds. The suspension was placed on a magnetic stirrer to allow washing for 24 hours.

The acetone was then vacuum filtered out to try to recover as much acetone as possible. The biochar was then washed with water and filtered using a total 800ml water to make the filtrate neutral pH.

When the filtrate was neutral, the biochar was placed in an oven at 100 °C to dry completely overnight. The dry biochar was then ground up to a fine powder and stored in zip bags.

Two simple magnetic separation tests were conducted to investigate whether iron-containing phases could be removed from the produced biochar. In the first test, a handheld magnet was placed directly in the dry biochar powder to determine if magnetic particles could be separated. In the second test, the biochar was dispersed in water to form a suspension, after which a magnet was placed on the outside of the beaker in an attempt to attract and separate the iron-containing particles.

3.2.1 Biochar Modification with Nitrogen

The biochar produced using the 1:1 red mud ratio and the biochar produced using the 1:3 NaOH activation were selected for nitrogen modification. 0.5g of each biochar sample was placed in separate autoclaves and mixed with 75mL of aqueous ammonia solution (25-28wt% NH_3). The autoclaves were tightly sealed and placed in an oven for 200°C for 48h to allow hydrothermal nitrogen modification of the biochar samples. After the treatment, the suspensions were vacuum filtered to recover the modified biochar. The collected samples were then dried in an oven at 100 °C overnight.

3.3 Analytical Methods

This section describes the analytical techniques used to characterize and analyze the produced biochar as well as the collected gas phase during pyrolysis. Several different methods were applied to investigate the morphology, elemental composition, specific surface area, adsorption & desorption performances of the materials, and the produced gases. The section presents experimental conditions for the analysis that were performed.

3.3.1 SEM & EDX Analysis

The biochar was placed on adhesive carbon tape and put into the Jeol JCM-7000 microscope (Tokyo, Japan) to perform Scanning Electron Microscopy (SEM) and Energy Dispersive X-ray Spectroscopy

(EDX) analysis. The SEM images were captured at three different magnifications (500x, 3000x, and 15000x), and the EDX was examined at 15kV acceleration voltage.

3.3.2 BET Surface Area Analysis

Small samples of the biochar were weighed and placed in tubes. The tube was placed in a vacuum and heated up to remove all water and other absorbed gases. After the sample cooled down, it was attached to the Micromeritics Gemini VII device and lowered into liquid nitrogen. Then, each sample was set on the device to be measured at 10 different points.

3.3.3 CO_2 Adsorption Measurement

Firstly, the biochar needed to be the suitable particle size to allow the gas flow to penetrate the particles of biochar in the colon. Therefore, the powdered biochar was pressed in a hydraulic hand press, Specac Ltd. (Orpington, UK), and then sieved to collect uniform biochar particles at a size of 0.7mm to 0.4mm.

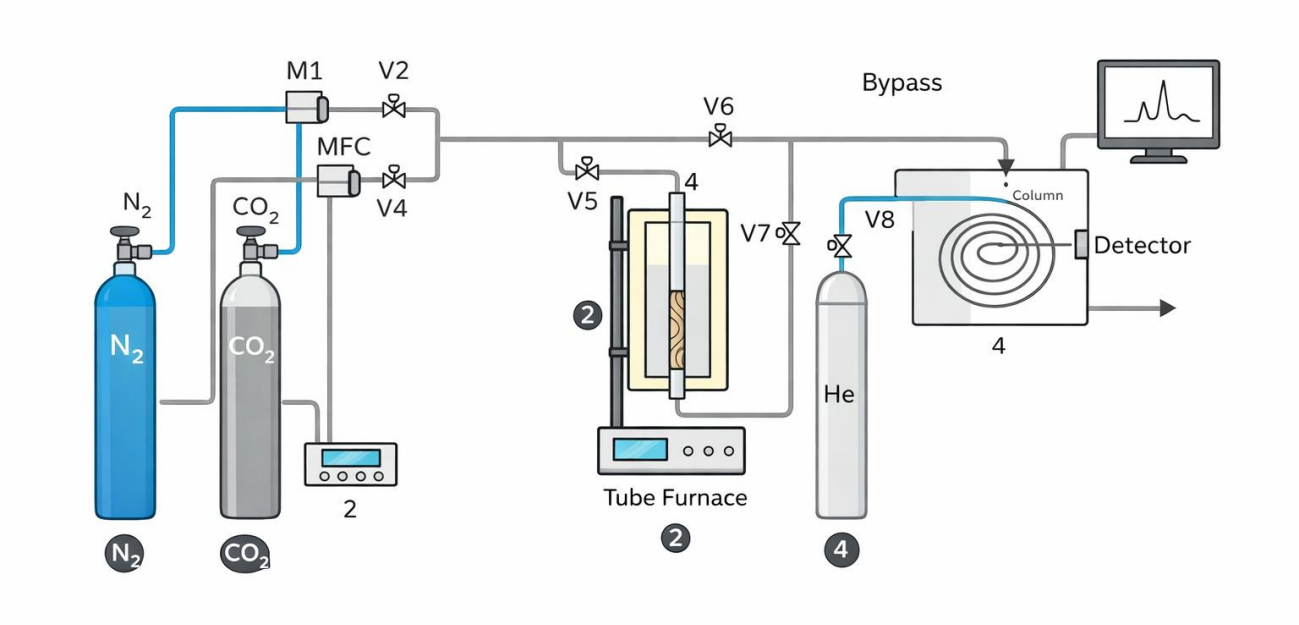

***Figure** 1. Equipment for CO_2 adsorption and desorption*

The biochar was then sealed in a glass colon by using a small piece of glass fiber on both ends. However, the isolation was not tightly packed since it could make the particles break into smaller pieces. This may have resulted in the gas not being able to pass through the colon.

The GC was turned on and once the oven reached 200 °C a continuous gas flow of nitrogen was passed through the system. The system was then flushed with only nitrogen until no impurities was found in the chromatograph.

After ensuring no impurities were left in the system, the nitrogen flow was redirected through the colon while it was simultaneously heated up to a temperature of 200 °C for 1 hour. This degassing process washed out the contaminants that may have been stuck inside the biochar's pores. The system was then cooled down by utilizing a fan to speed up the process. While the system was

cooling down blank GC runs were performed to ensure that any potential contaminants from the degassing got flushed out. At the same time, the gas flow rate of nitrogen and carbon dioxide was determined to confirm that correct amount nitrogen-to-carbon dioxide ratio was prevalent. The regulation ratio was set at 10% CO_2 and 90% N_2 in the mixed gas flow. The total flow rate varied between 94 ml/min and 85,2 ml/min due to how easily the flow could go through the material in the colon.

When the flow was regulated to the wanted ratio, the GC was flushed with nitrogen until no carbon dioxide from the regulation was shown in the chromatogram. The carbon dioxide and nitrogen were then turned on to create the bypass Three bypasses were created to ensure that the system and flows were consistent.

The system was flushed again with nitrogen to remove all the carbon dioxide that might have gotten stuck in the system. The adsorption then begun by letting the mixed regulated gas flow through the biochar packed colon. The GC ran until the carbon dioxide peak was unchanged or until it was the same as the reference CO_2 peak.

The system was then flushed again until no carbon dioxide peak appeared to ensure no carbon dioxide was left in the system. The desorption begun by heating up the colon to 150 degrees for 3 hours. During these three hours, the GC was continuously measuring and was stopped when the carbon dioxide peak disappeared.

3.3.4 Gas Phase Analysis

Firstly when analyzing the gasses produced during the different pyrolysis's the Gas Chromatograph was turned on with the settings shown in table 1.

Detector	TCD
Temperature Detector	200°C
Injection Chamber Temperature	40°C
Column Flow	20ml/min
Gas Injected	0.5ml
Running Time	14.35min
Carrier Gas	Helium

***Table** 1. The settings used for the gas chromatography.*

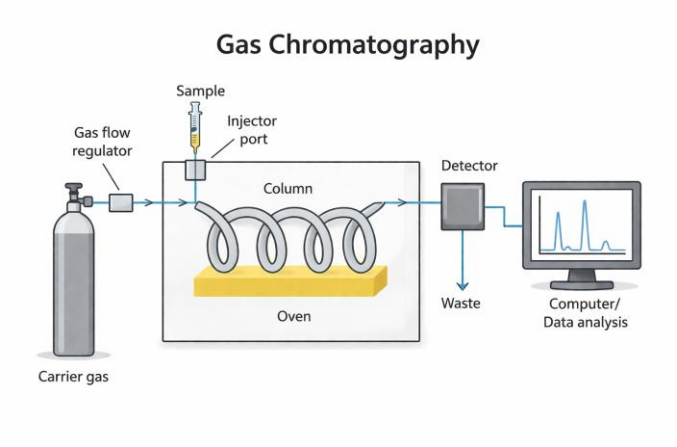

***Figure 2**. The Gas Chromatography System*

When the detector TCD temperature reached 200°C the sample was prepared. During the Gas Phase analyzis the same GC was used however instead of an online sampling by a sampling loop attached to the GC we manually injected our sample. A gas tight syringe was inserted into the sample bag and the gas was mixed by repeatedly drawing and reinjecting the gas to ensure a homogeneous composition (see figure 2). The syringe was then filled with 0,6 ml, after which 0,11 ml was reinjected to the bag. This resulted in a final sample volume of 0,5 ml. The syringe was inserted into the injector port and the sample was injected. The gas chromatography run was conducted for 18 14,35 min after which the chromatographic peaks were identified based on their retention times and their appearance.

3.4 Calculation

In this section, the calculations used to quantify experimental parameters are described. These include yield calculations, gas phase analysis, and adsorption–desorption calculations. The methods applied provide a basis for evaluating the material performance and comparing the different activation approaches.

3.4.1 Yield Calculation

Different yield values were calculated in order to obtain a broader understanding of the method. Two types of yields were evaluated: the yield directly after pyrolysis and the yield after the washing procedure.

All yields are reported as percentage values and were calculated using the following math equations:

$$Yield\ After\ Pyrolysis = \frac{Biochar}{Biomass + Red\ Mud}$$

$$Yield\ After\ Washing = \frac{Washed\ Biochar}{Biomass + Red\ Mud}$$

For NaOH-activated biochar, most of the NaOH could be washed away. Therefor the yield was calculated by the following equation.

$$Yield\ After\ Washing = \frac{Washed\ Biochar}{Biomass}$$

In these equations, *biochar* refers to the mass of solid dry products obtained right out of the pyrolysis oven. *Washed Biochar* refers to the recovered mass after the acetone washing, water washing and final filtration procedures were complete. *Biomass* represents the initial dry mass of acacia wood and *Red Mud* corresponds to the initial dry mass of red mud added during activation.

3.4.2 Gas Phase Calculations

For each biochar sample and temperature range replicates were made. From these replicates the average peak area was calculated and used to determine the gas concentrations.

The relationship between peak area and concentration was defined using the calibration equation:

$$A_{standard} = mx$$

where $A_{standard}$ is the standard peak area for the component, x is the percentage concentration of the component and m is the slope of the calibration curve. Value A and x was given to us based on the standard.

Gas	Concentration Percentage	$A_{standard}$	m
Hydrogen	30%	0,2857	0,95
Nitrogen	99,90%	120,2411	120,36
Methane	35%	17,8079	50,88
Carbonmonoxide	10&	6,9777	69,78

Tabell 2: *Presents the different percentage concentrations of each gas, their standard peak area and the calculated slope of the calibration curve.*

The average concentration was then calculated as:

$$C = \frac{A_{Average} * x}{A_{standard}}$$

The calculated concentrations were used to construct bar chart. Each chart represents a specific component (e.g. hydrogen). The x-axis corresponds to the temperature ranges while the y-axis represents the concentration. For each temperature range three bars were shown corresponding to the different biochar samples.

3.4.3 CO_2 Adsorption & Desorption Calculations

When all carbon dioxide peak areas had been recorded, the CO_2 concentration was calculated. Both the relative concentration (as a percentage of the total flow) and the absolute concentration were determined.

The percentage concentration was calculated as:

$$C_{Percentage} = A_{CO2\ Peak} * \frac{S_{Peak}}{x} \quad (\%)$$

Where, $A_{CO2\ Peak}$ is the peak area obtained from the gas chromatography analysis for each adsorption and desorption experiment, and S_{Peak} is the standard peak area determined as the average from at least three bypasses. The variable x represents the known CO_2 fraction in the gas feed which was around 10%.
The gas flow rate was measured using a bubble flow meter and then calculated using:

$$r = \frac{V*60}{t}$$

Where r is the volumetric flow rate (L/min), V is a chosen volume (L), and t is the time (s) required for the gas to reach that volume. In our case we had V as 0,5 ml.

Using the flow rate, the experimental CO_2 fraction in the total flow was calculated as:

$$x_{experimental} = \frac{r_{CO2}}{r_{Total}}$$

The absolute concentration was obtained from:

$$C_{CO2} = A_{CO2\ Peak} * \frac{S_{Peak}}{x_{experimental}}$$

These concentrations were subsequently used to determine the amount CO_2 that had been adsorbed in each run. The adsorbed amount was calculated by numerical integration using the trapezoidal rule:

$$S_{adsorp} = \sum_0^t [\frac{1}{2} * (2C_{max} - (C_i + C_{i+1})) * \Delta t$$

Where S_{nhp} was the total amount adsorbed, C_{max} was the highest concentration adsorbed amongst all the runs. C_i and $C_{i+1}$was the concentration at different times and where Δt was the time interval between the measurements of concentration.

The same calculations applied for desorption when quantifying the concentration of CO_2. However when calculating the total amount desorbed this equation was used:

$$S_{desorp} = \sum_0^t [\frac{1}{2} * (C_i + C_{i+1}) * \Delta t$$

Then the total amount adsorbed and desorbed amounts were obtained by summing up all the concentrations over the entire time.

Finally, the adsorption/desorption capacity was calculated by converting it from ppm*min to mmol/g:

$$q = \frac{r_{tot} * 10^{-6} * S}{22{,}4 * m}$$

Where q is the adsorption or desorption capacity (mmol/g), r_{tot} is the total integrated CO_2 signal (ppm*min), 10^{-6} is the conversion factor from ppm to molar fraction, S is the volumetric gas flow rate (L/min), 22.4 is the molar volume of an ideal gas at standard conditions (L/mol), and m is the mass of the adsorbent (g).

4 Results & Discussion

This chapter presents the experimental results obtained in this study and provides interpretations of the findings. The results are discussed in relation to the objective of the thesis and existing literature.

4.1 SEM-EDX Morphology and Elemental Composition of Raw Material

In this section, the morphology and elemental composition of the raw materials used in this study are presented and discussed. SEM-EDX analysis was performed on both acacia wood and red mud in order to characterize their surface structure and composition prior to pyrolysis. This provides a reference point for evaluating the changes during the biochar production.

4.1.1 **Raw Acacia Wood**

Raw Acacia Wood Elemental Composition

Element	**Mass %**	**Atomic %**
C	54.52 ± 5.66	62.58 ± 5.03
O	41.22 ± 5.45	36.88 ± 4.82
K	3.23 ± 3.02	1.47 ± 1.36
Mg	0.27 ± 0.42	0.22 ± 0.34
Cl	0.11 ± 0.19	0.07 ± 0.13
Al	0.04 ± 0.07	0.03 ± 0.05

Table 3. *Elemental surface composition of raw acacia wood determined by SEM-EDX analysis. Values represent mean ± standard deviation from multiple measurement points.*

SEM–EDX analysis of the raw acacia wood biomass showed that the material consisted primarily of carbon and oxygen, with somewhat consistent potassium contents ranging between 0-7 mass%. In some localized regions, small amounts of magnesium, chlorine, and aluminium were detected, although these were not consistently present across all measurement points. The presence of potassium is noteworthy, as previous studies (e.g., Synthesis and Characterization of Biochars and Activated Carbons Derived from Various Biomasses) have reported that naturally occurring potassium in biomass can promote activation processes and enhance both specific surface area (SSA) and CO_2 adsorption performance. Cl and Al are minor components, due to the lesser accuracy of EDX method, these elements can be considered uncertain.

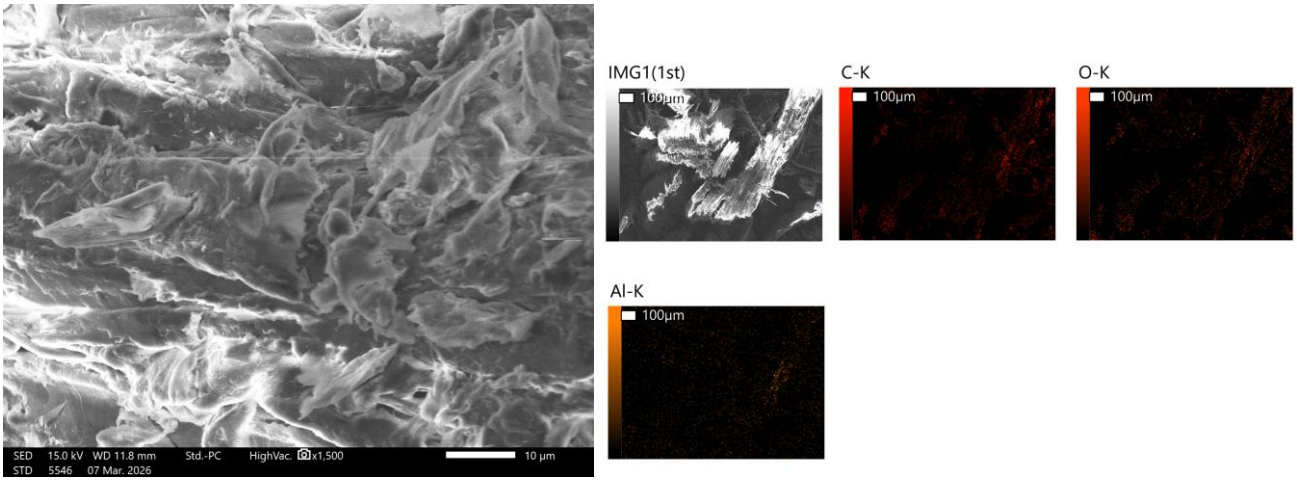

***Figure 3**. SEM 1500x 15kV Photo & Mapping of Raw Acacia Wood*

4.1.2 **Raw Red Mud**

Element	**Mass %**	**Atomic %**
C	3.81 ± 1.26	7.00 ± 2.35
O	33.94 ± 0.94	54.86 ± 0.95
Na	4.17 ± 0.36	4.52 ± 0.09
Al	9.14 ± 1.41	9.28 ± 0.55
Si	4.47 ± 0.47	3.89 ± 0.48
Fe	42.12 ± 1.48	19.06 ± 0.58

***Table 4.** Elemental composition of raw red mud determined by SEM-EDX analysis. Values represent mean ± standard deviation from multiple measurement points.*

The EDX analysis of the raw red mud confirmed the presence of multiple inorganic components, including measurable sodium concentrations of approximately 4–5 mass%. Sodium is commonly associated with chemical activation processes and may contribute to activation effects during thermal treatment. However, what the chemical composition of sodium as well as the actual availability of the sodium under the pyrolysis in this study remain uncertain. Fe is the main composition of red mud, together with some Si and Al.

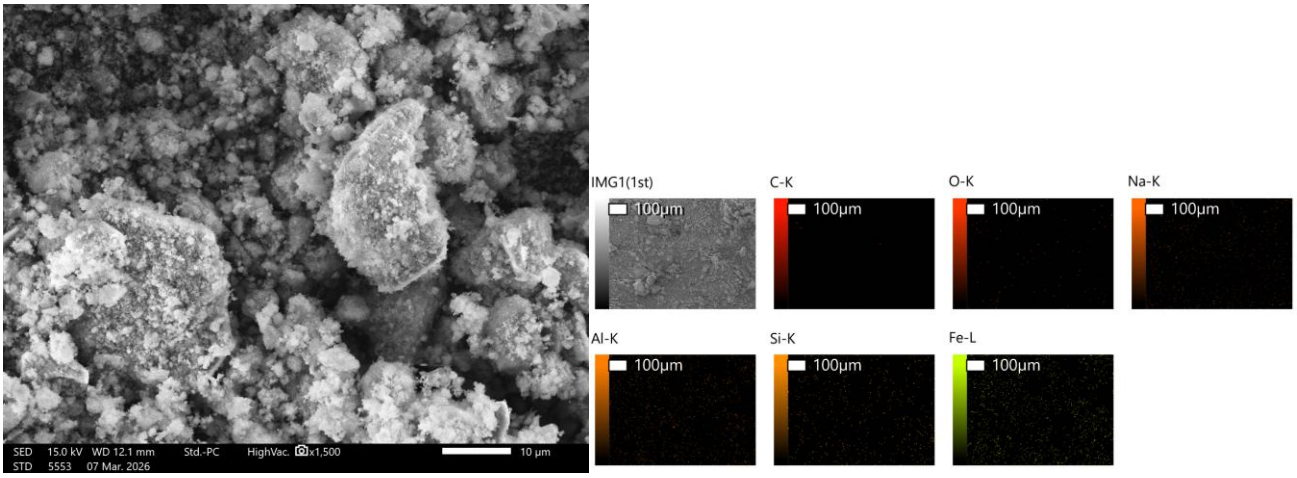

***Figure 4**. SEM 1500x 15kV Photo & Mapping of Raw Red Mud*

4.2 SEM-EDX Morphology and Elemental Composition of Biochar

In this section, the morphology and elemental composition of the biochar produced in this study are presented and discussed. SEM-EDX analysis was performed on all different samples of biochar, including the different red mud ratios, NaOH-activated biochar, and nitrogen-modified biochar. The analysis provides insight into the surface structure and composition of the materials, allowing comparison between the different activation methods and modification approaches.

4.2.1 Effect of Red Mud Ratios

Comparing the EDX results of the two ratios, a substantially higher Fe and overall mineral content are observed in the 1:3 sample. Correspondingly, the relative carbon content is significantly lower compared to the 1:1 material. The relatively large standard deviations observed for several elements indicate a heterogeneous distribution of mineral phases across the biochar surface. Ca, K, S are minor components, due to the lesser accuracy of EDX method, these elements can be considered uncertain. Comparing the element composition of the raw biomass, raw red mud, and the produced biochar reveals clear changes in the composition after pyrolysis. The carbon content in the biochar is significantly lower than that of the raw biomass. At the same time, the relative iron content becomes more prominent in the biochar samples. Noticeably, elements such as Si, Al, and Na showed a lower relative percentage of the composition compared to the raw red mud. This may be due to the fact that Si and Al may react with NaOH in read mud at high temperature to form Na2SiO3 and NaAlO2 with may be filtered out of the solid during the washing process. NaOH may also react with C in biomass to form Na2CO3 which is also lost during the washing process. The presence of Ti may be due to the increase of it content, which is originated from red mud but is in too low content to be detected in the raw read mud, due to the decrease of Al, Si content.

Element	Ratio 1:1 Mass%	Ratio 1:3 Mass%	Ratio 1:1 Atomic%	Ratio 1:3 Atomic%
Fe	40.48 ± 17.62	50.49 ± 19.08	25.55 ± 15.87	29.63 ± 16.88
O	25.59 ± 8.12	29.68 ± 11.62	38.02 ± 13.48	39.48 ± 15.23
C	27.04 ± 18.96	13.77 ± 11.25	30.37 ± 26.39	16.68 ± 14.33
Al	4.45 ± 2.01	3.53 ± 1.81	4.68 ± 3.66	3.49 ± 2.49
Si	1.86 ± 0.83	1.49 ± 0.62	1.63 ± 0.90	1.31 ± 0.57
Ti	3.12 ± 1.10	3.75 ± 1.21	1.84 ± 0.79	2.12 ± 0.87
Na	1.28 ± 0.52	2.18 ± 0.94	1.66 ± 0.77	2.83 ± 1.25
Ca	0.99 ± 0.46	0.72 ± 0.39	0.67 ± 0.33	0.48 ± 0.25
K	0.21 ± 0.16	0.38 ± 0.27	0.20 ± 0.14	0.36 ± 0.22
S	0.26 ± 0.22	0.41 ± 0.31	0.18 ± 0.13	0.29 ± 0.21

Table 5*. Compiled SEM-EDX results showing the mean elemental composition (mass% and atomic%) and the standard deviation of biochar samples for activation ratios 1:1 and 1:3. Values represent average measurements from multiple analysed regions.*

SEM images and elemental mappings further confirm these findings. The surface morphology of both samples is influenced by mineral phases; however, the 1:3 sample shows a more pronounced

dominance of iron-rich regions. In this material, iron-containing particles appear more uniformly distributed across the surface, whereas the 1:1 sample retains comparatively larger carbon-rich areas. These results indicate that increasing the red mud ratio leads to greater mineral prevalence at the biochar surface and a reduced exposure of carbon-rich domains.

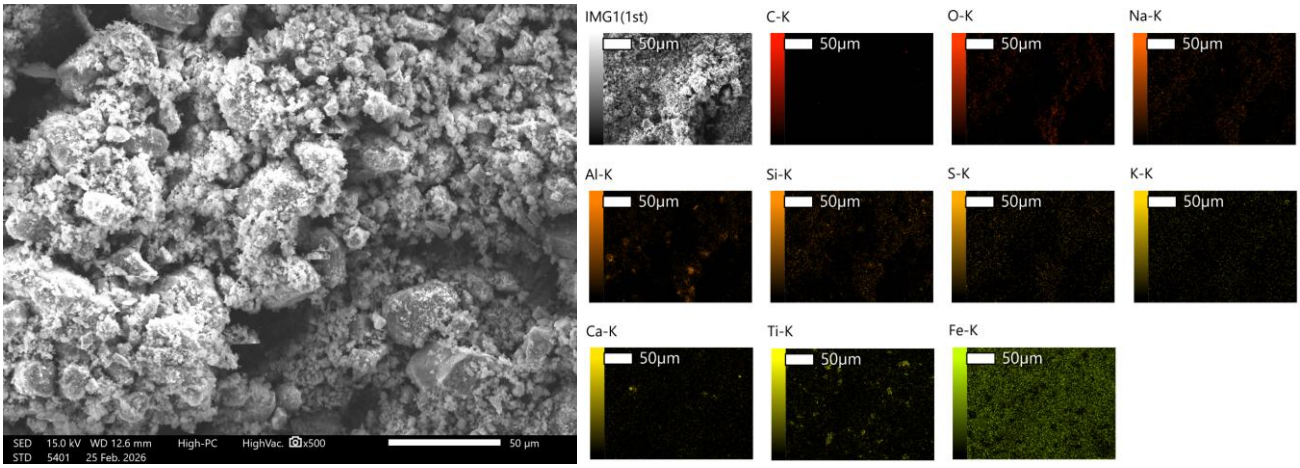

***Figure 5**: SEM 500x 15kV Photo & Mapping of 1:3 Ratio Sample*

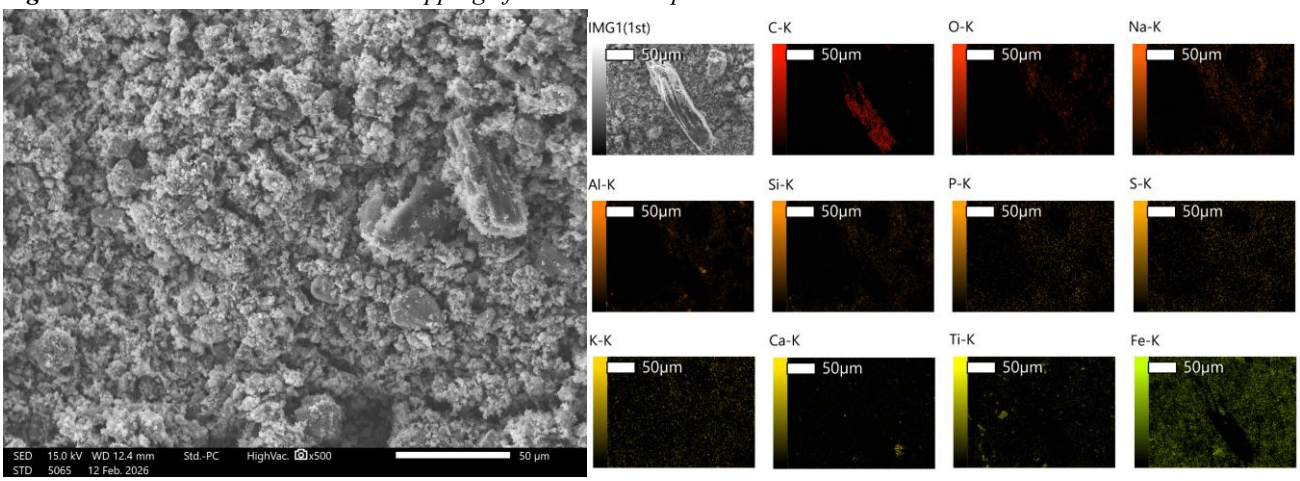

***Figure 6.** SEM 500x 15kV Photo & Mapping of 1:1 Ratio Sample*

This outcome is expected, as a higher amount of red mud introduced prior to pyrolysis results in a larger fraction of non-volatile inorganic oxides remaining in the solid residue. The reduction in relative carbon content can partly be explained by a dilution effect, where increasing mineral mass lowers the proportional carbon fraction. In addition, the catalytic effects of metal oxides during pyrolysis may promote carbon conversion to gaseous products, further reducing the fixed carbon content in the final material. Overall, the inorganic fraction plays a decisive role in defining the chemical identity of the produced biochar.

Studying the morphology with SEM-EDX, we also observe that the solid residue from the mineral composition becomes dominant on the surface of the biochar. The SEM imaging and elemental mapping further confirm that a higher ratio of red mud will be even more dominant on the surface of the biochar. Interestingly, some heterogeneity could be seen during the SEM-EDX analysis. Pure parts of carbon could be found during examination, and generally more often in the 1:1 ratio. This could be explained by non-uniform impregnation of red mud and biomass prior to pyrolysis, as well as localized aggregation of mineral particles. The decrease in carbon content observed in the biochar

samples can likely be connected to the thermal decomposition of the biomass during pyrolysis, where the volatile compounds containing carbon such as CO_2, CO and hydrocarbons are released. The enrichment of the iron in the biochar is expected since the mineral phases from the red mud remain, while organic compounds from the biomass are partially volatilized. This results in a higher relative concentration of inorganic compounds in the final biochar.
In contrast, the lower relative percentages of Si, Al, and Na may partly be related to the heterogeneous distribution of the mineral phases, since the SEM-EDX only measures the surface of the sample.

4.2.2 **Comparison with NaOH-activated Biochar**

The SEM-EDX and elemental composition analysis of the NaOH-activated biochar show a big difference compared to the red mud activated biochar. Most notably, a higher amount of carbon is present in the biochar because different from the red mud, NaOH was removed during washing after the pyrolysis. Considerably lower amounts of minerals like Fe, Al, and Si are still present, which indicates that the surface of NaOH-activated biochar is dominated by carbon rather than inorganic mineral phases. Fe, Al and Si may be contaminants from the ceramic boats. Lower amounts of Na are also observed, which suggests that most of the remaining Na after pyrolysis was successfully washed away during the washing procedure, but not completely.

Element	**Mass % (mean ± SD)**	**Atomic % (mean ± SD)**
C	67.24 ± 1.65	77.76 ± 3.98
O	18.72 ± 2.74	16.42 ± 2.28
Na	2.43 ± 1.45	1.46 ± 0.89
Mg	0.06 ± 0.11	0.03 ± 0.05
Al	2.79 ± 0.77	1.88 ± 0.59
Si	3.24 ± 1.50	1.80 ± 1.16
Ca	0.49 ± 0.56	0.17 ± 0.19
Fe	1.16 ± 1.39	0.28 ± 0.33

***Table 6**. Average elemental composition of NaOH-activated biochar determined by SEM–EDX analysis. Values represent the mean of four measurements ± standard deviation.*

In contrast, the red mud activated biochar exhibits a much higher abundance of mineral elements, particularly iron which remains solid during pyrolysis and therefore strongly influences the surface of the produced material. The higher carbon content observed in the NaOH-produced biochar suggests that this activation method produces a material with a larger fraction of exposed carbon surfaces, whereas red mud derived biochar forms a type of mineral-carbon composite structure.

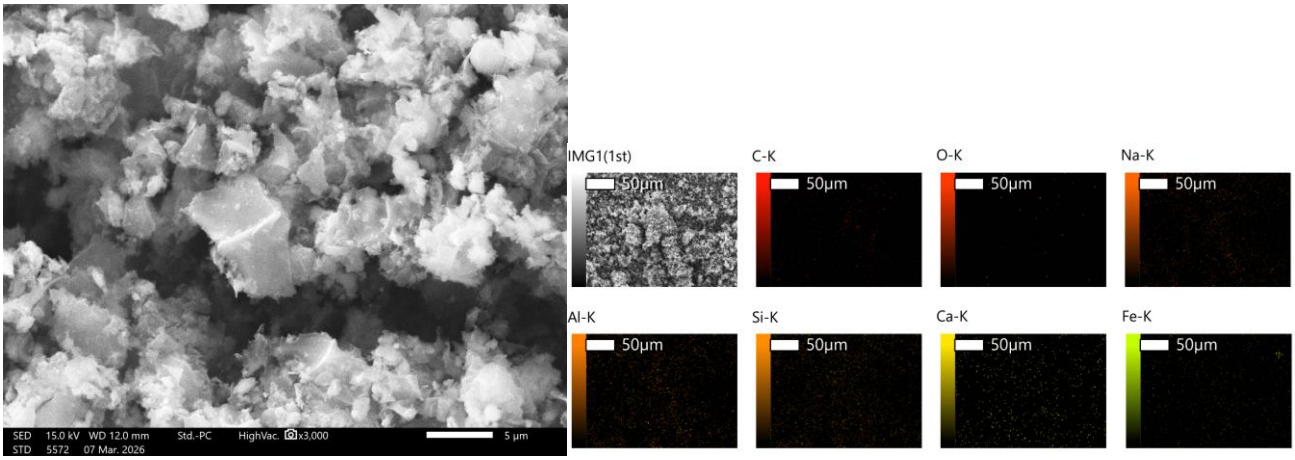

Figure 7. *SEM 3000x 15kV Photo & Mapping of 1:3 NaOH Ratio Sample*

The differences in surface composition between the two activation agents are expected. The influence on the adsorption properties of the activation agents has to be evaluated by BET analysis and CO_2 adsorption measurements.

4.2.3 **Nitrogen Modification Biochar**

SEM-EDX analysis of both nitrogen-modified biochars (1:1 red mud activated and 1:3 NaOH activated) revealed only small signals of nitrogen in very localized areas. In larger elemental mapping areas, nitrogen could not be detected clearly.

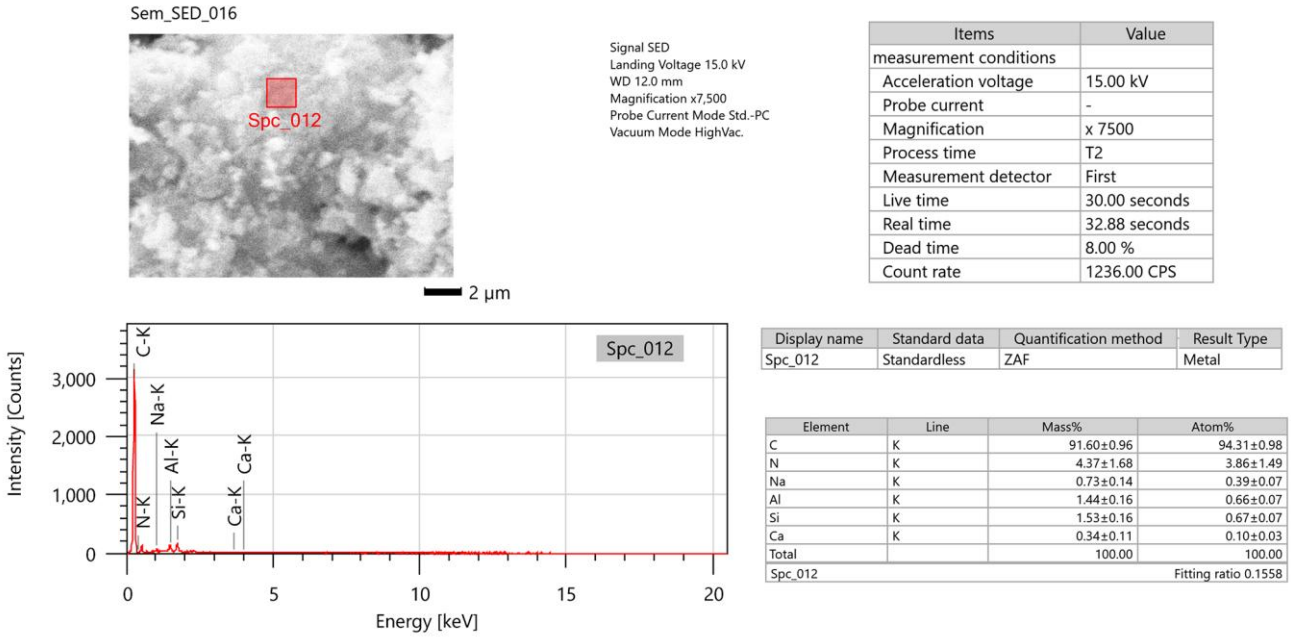

Items	Value
measurement conditions	
Acceleration voltage	15.00 kV
Probe current	-
Magnification	x 7500
Process time	T2
Measurement detector	First
Live time	30.00 seconds
Real time	32.88 seconds
Dead time	8.00 %
Count rate	1236.00 CPS

Display name	Standard data	Quantification method	Result Type
Spc_012	Standardless	ZAF	Metal

Element	Line	Mass%	Atom%
C	K	91.60±0.96	94.31±0.98
N	K	4.37±1.68	3.86±1.49
Na	K	0.73±0.14	0.39±0.07
Al	K	1.44±0.16	0.66±0.07
Si	K	1.53±0.16	0.67±0.07
Ca	K	0.34±0.11	0.10±0.03
Total		100.00	100.00
Spc_012			Fitting ratio 0.1558

Figure 8. *EDX of 1:3 NaOH-activated, ammonia-treated biochar, showing the presence of nitrogen.*

This might be because of the low detection sensitivity of EDX for light elements such as nitrogen, and adding nitrogen through hydrothermal treatment is considered a mild modification method that often results in a low percentage of impregnation, while still being a good way of getting a high dispersity of nitrogen, which in contrast can make detection by EDX even more difficult. Hydrothermal ammonia treatment did not appear to change the overall morphology of the biochar samples, as elemental compositions and SEM images showed surfaces similar to unmodified

biochar, with dominating mineral phases for the red mud activated samples and still the presence of Na for the NaOH activated samples, and although some small areas of nitrogen could be detected, the overall morphology stayed unchanged.

4.3 Biochar Yield

For the biochar produced with red mud as an activation agent, two different yields were calculated: one directly after pyrolysis and one after the complete washing procedure. In the case of the NaOH-activated biochar, only the final yield after washing was considered relevant, since the washing steps remove most of the remaining NaOH from the material.

The red mud activated samples showed relative consistency. Particularly examining the yield directly after pyrolysis. The ratio 1:3 resulted in yields of approximately 68-70%, while the 1:1 ratio produced yields around 54-55%. The large yield of 1:3 can be attributed to the simple fact that there is a higher amount of red mud which can't be converted during pyrolysis. A somewhat larger variation was observed after the washing procedure. This variation may partly be attributed to procedural refinement, including improved filtration efficiency in later experiments. The later ones were done more efficiently using fewer filter papers, which in turn means smaller losses. The pre-wash yields calculated from red mud replicates experiments are approximately the same, confirming the reproducibility of the pyrolysis.

The recovered yield for the NaOH-activated biochar was substantially lower compared to the red mud activated samples. From 15g of raw biomass, only 0.6g of biochar could be collected after the washing procedure. However, since this value is lower than expected, it should be interpreted with caution and may reflect material losses during pyrolysis, washing, or filtration rather than the actual yield of the NaOH activation route.

Another possible explanation is that NaOH reacts with carbon during thermal treatment, leading to the formation of intermediate sodium compounds such as Na_2CO_3. Since these compounds are highly water-soluble they are removed during the washing procedure. In contrast, the mineral oxides present in red mud do not undergo the same type of reaction and therefore remain incorporated within the carbon structure after washing. This may be the reason why NaOH activated biochar exhibited a substantially greater mass loss during the washing procedure compared to the red mud samples.

However, red mud also contains small amounts of NaOH which may react similarly during pyrolysis and subsequently be removed during washing. This could contribute to the observed mass loss after washing and thereby lower the final biochar yield. Since 1:3 red mud ratio contains a larger amount of red mud and consequently a higher amount of NaOH, this may explain the greater reduction in mass and yield for the 1:3 red mud sample compared to the 1:1.

Ratio	Run	Initial Mass (g)	Dry Biochar (g)	Yield Before Wash (%)	Final Yield (%)
1:3 Red Mud	#1	60	33.7	70.47	56
	#2	24	14.85	68.75	62
	#3	24	15.3	70.42	64

Ratio	Run	Initial Mass (g)	Dry Biochar (g)	Yield Before Wash (%)	Final Yield (%)
1:3 Mean ± SD				**69.88 ± 0.98**	**60.67 ± 4.16**
1:1 Red Mud	#1	30	12.7	54.57	42
	#2	12	5.8	55.00	48
	#3	12	6.5	55.00	54
1:1 Mean ± SD				**54.86 ± 0.25**	**48.00 ± 6.00**
1:3 NaOH	#1	15	0.6	**-**	**4**

***Table** 7: Yield results for different ratios, activation agents.*

4.4 Gas Phase Analysis

In this section, the gas phase composition obtained during pyrolysis is presented and discussed. The analysis is divided into three temperature ranges (400–500 °C, 500–550 °C, and above 550 °C) to evaluate how gas formation evolves with increasing temperature. The results are compared for the different red mud activation ratios as well as for the NaOH-activated biochar.

4.4.1 Unknown Gas

Table 7 shows the different retention times that matches the standard retention time for hydrogen. According to the table the presence of hydrogen should be available in almost all pyrolysis's with red mud while none is present in the sodium hydroxide.

Retention Time		1:1 Red Mud	1:3 Red Mud	1:3 NaOH
	Standard	Hydrogen 1.18	Hydrogen 1.18	Hydrogen 1.18
	400-500°C	1.182 1.185 -	1.185 - -	-
	500-550°C	1.202 1.185 -	- - -	-
	550+°C	- - 1.185	1.235 - 1.185	-

***Table 8**: Only based on the retention times and represents the retention time of hydrogen for each replica and each temperature range*

However the table is only based on the times without actually analyzing the peaks. After observing the different peaks we can conclude that these peaks are indeed not hydrogen. The reason for this assumption is because the hydrogen peak is different. In contrast with other peaks hydrogen peaks goes down. In conclusion none of the peaks was hydrogen. We can only conclude that these peaks are some kind of impurities.

One possible reason for their occurrence is that only 0,5 ml was injected in the system meaning that there could have been an unequal distribution of the gas in the bag. Efforts were made to avoid this by repeatedly drawing and injecting it using a gas-tight syringe. This meant that the gas was manually mixed to reach a homogenous mixture.

4.4.2 Methane Gas

In the Figure 10 it can be observed that in the temperature range 400-500°C all three pyrolysis shows similar methane concentrations. In the range 500-550 °C, the 1:1 red mud and the 1:3 sodium hydroxide samples shows significantly higher methane concentrations compared to the 1:3 red mud

sample. One possible explanation is that a higher red mud ratio may lead to pore blockage, which limits the formation of intermediates that are usually produced around these temperatures. The intermediates that would otherwise produce methane can instead be promoted to convert into other gaseous products such as CO. At temperatures higher than 550 degrees we can see much higher methane concentration in the sodium hydroxide compared to the red mud ones. One possible explanation is that NaOH reacts with the carbon during pyrolysis promoting the formation of gaseous compounds. Since 1:3 red mud contains larger amounts of red mud and consequently a higher amount of NaOH, this may contribute to the higher formation of methane observed compared to the 1:1 red mud sample.

One particular trend that is similar across all experiments is that the concentration of methane increases with increasing temperatures. This is consistent with theoretical expectations since the gas production increases with temperature due to progressive thermal decomposition of the pseudo components of the biomass. At temperatures above 550°C cellulose, hemicellulose and lignin has majorly started to decompose and gas formation becomes the dominant reaction pathway, which is why in the diagram we can see that for all the experiments the concentration increases at higher temperatures.

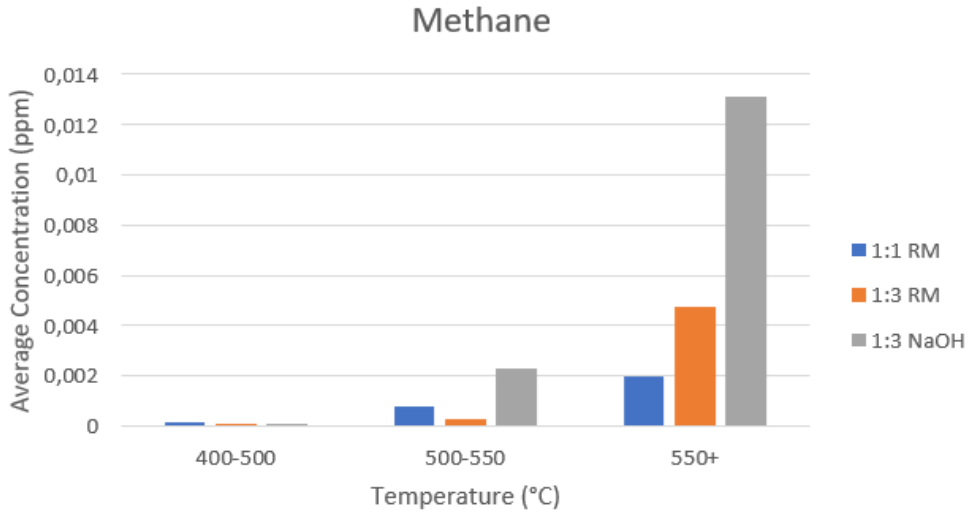

Figure 9. *The average concentration methane captured from different ratios and activation agents during pyrolysis*

4.4.3 Carbon monoxide Gas

With carbon monoxide we can observe based on figure 6 that at lower temperatures the blocks do not differ much. However, both red mud attempts is producing higher concentrations then sodium hydroxide. This is even more clear when the temperatures rises since the blocks of red mud significantly increase while the carbon monoxide concentration in the sodium hydroxide doesn't change significantly. One core explanation that has been brought up before in the thesis is that red mud has catalytic properties. And with higher ratio of red mud more active sites are available. These catalytic properties often converts oxygen containing intermediates into carbon monoxide. Also, Red mud contains a large amount of Fe_2O_3 which can react with carbon to form Fe_3O_4 and CO. Since the 1:3 red mud sample contains more Fe_2O_3 consequently the formation of carbon monoxide is higher compared to 1:1 red mud.

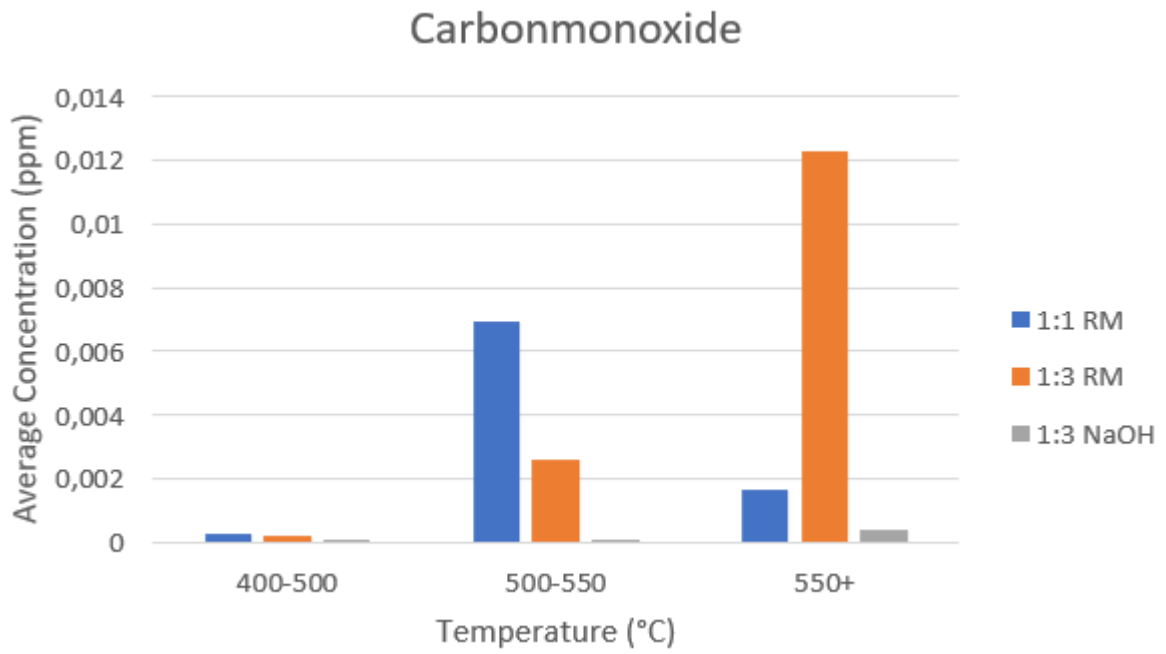

Figure 10. *The average concentration CO captured from different ratios and activation agents during pyrolysis*

As carbon monoxide can easily be oxidized to carbon dioxide and is highly toxic at elevated concentrations, its formation during pyrolysis is undesirable and should be minimized. This suggests that the use of red mud as an activation agent is less favourable when evaluated solely based on this aspect.

4.5 Surface Area Analysis (BET)

BET surface area analysis revealed clear differences in specific surface area (SSA) between the different ratios as well as the different activation agents. For red mud activated biochar, the lower ratio of 1:1 resulted in a higher SSA of 94m²/g, whereas the higher ratio of red mud 1:3 showed a lower SSA of 74m²/g.

Increased red mud content may affect pore development in multiple ways. The mineral particles can act as structural templates that influence gas evolution and pore formation during thermal treatment. At the same time, excessive mineral content may occupy or block pore structures reducing the specific surface area available for adsorption. The measured surface area therefore reflects a balance between pore formation and pore obstruction.

In contrast, the NaOH-activated biochar resulted in a significantly higher SSA of 313m²/g. The large difference was expected since NaOH is used as a common activator for porous carbons. It's known to promote strong chemical reactions with the carbon matrix to enhance pore formation. These results further confirm this and indicate that NaOH activation is an effective way of producing porous carbon.

Activation agent	**Ratio (Biomass : Activator)**	**Sample ID**	**BET SSA (m²/g)**
Red Mud	1:1	#1	94
Red Mud	1:3	#1	74

Activation agent	Ratio (Biomass : Activator)	Sample ID	BET SSA (m^2/g)
NaOH	1:3	#1	313

Table 9. *Presents the SSA of different ratios and activation agents.*

Specific Surface Area is a strong indicator of CO_2 adsorption efficiency, but more analysis methods like CO_2 adsorption and desorption are needed to get a clearer and more honest result. For example, it should be noted that the presence of the residual mineral phases in the red mud activated samples may dilute the measured surface area when expressed per gram of total material.

4.6 CO_2 Adsorption Performance

This chapter presents the results of the biochar's adsorption-desorption abilities carbon dioxide. It also contains comparison between 1:1 Red Mud activation and 1:3 NaOH activation to produce biochar.

4.6.1 1:1 Red Mud

The observed adsorption behavior indicates that the material initially captures CO_2 effectively. This is indicated by the zero outlet concentration at the beginning of the adsorption curve. As time increases the CO_2 concentration rises which suggests that the biochar gradually becomes saturated and that the gas begins to pass through the system. However the initial low outlet concentration may also be influenced due to the time required for the gas to pass through the system. Which can mean that when the experiment has begun the CO_2 has not yet had the time to reach the injection point. This may result in delay in time.

During desorption we can clearly see that in the beginning, the CO_2 is released rapidly and then steady decreasing until it reached 0. This indicates that the desorption was efficient.

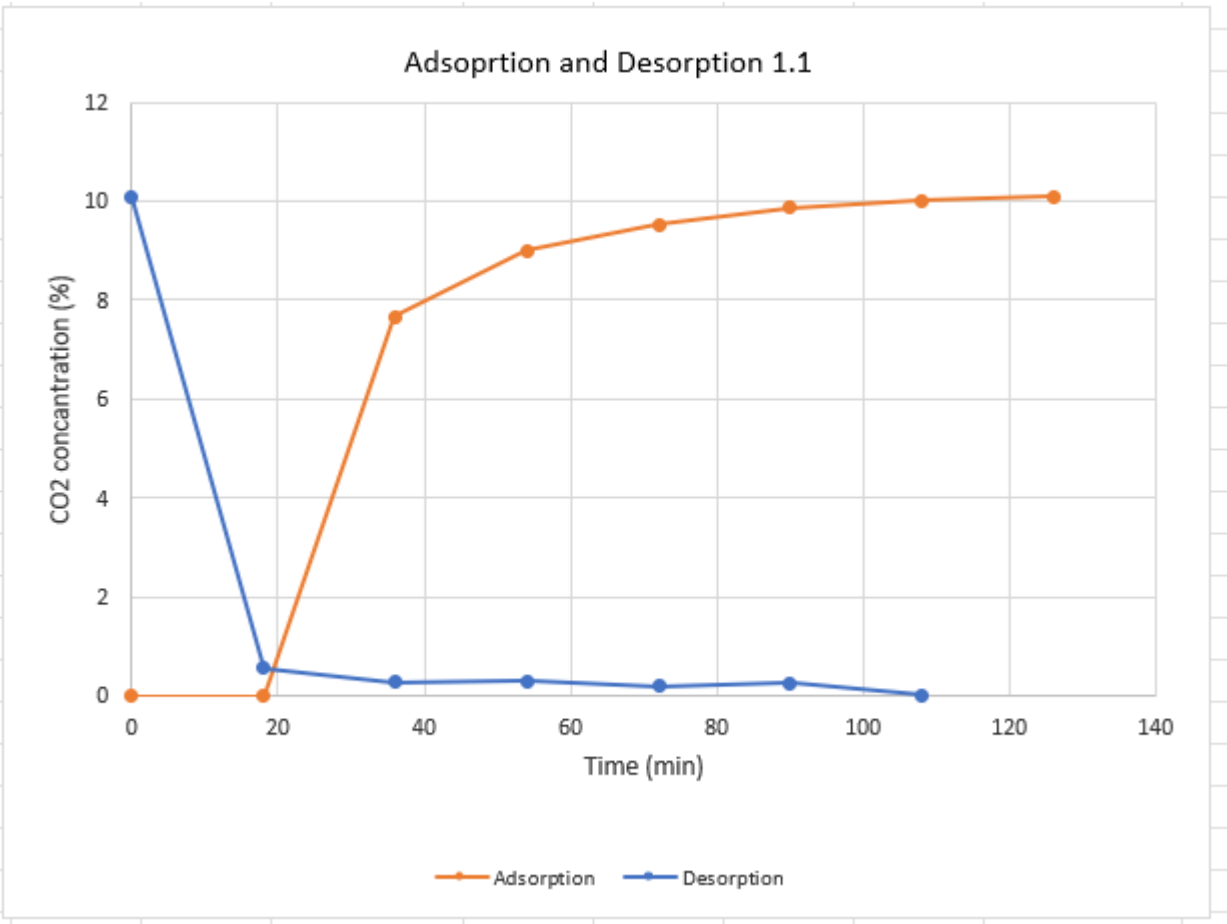

Figur 11. CO_2 *Adsorption and desorption curves for biochar derived fopm 1:1 Red mud ratio.*

However table 9 indicates that total quantity of desorbed CO_2 is low. This can be observed by the big difference between the adsorption quantity and the desorption quantity. This means that CO_2 was captured tightly inside the biochar but regeneration of the biochar was difficult. One main reason may be that red mud has a lot of catalytic sites causing the carbon dioxide to bond more stronger to these, making it more difficult to break these bonds. One way that could make the regeneration higher would be desorption at higher temperature. Since higher temperature leads to more bonds breaking it could desorb higher quantities from the saturated biochar.

Adsorption	0.0259 (mmol/g)
Desorption	0.0006 (mmol/g)

Table 10*. Present the adsorption-desorption for 1:1 Red Mud activated biochar.*

4.6.2 1:3 NaOH

The observed adsorption behavior indicates that the material shows limited CO_2 capture at the beginning of the experiment. This is reflected by the paid increase in the outlet CO_2 concentration, which reaches approximately 9% within a short period of time. This suggests that the biochar becomes saturated quickly and that CO_2 passes through the system with minimal adsorption.

During desorption, it can be observed that the CO_2 concentration decreases indicating that CO_2 is released from the material. However the relatively low concentration during the desorption phase suggests that only a limited amount of CO_2 was adsorbed in the first place.

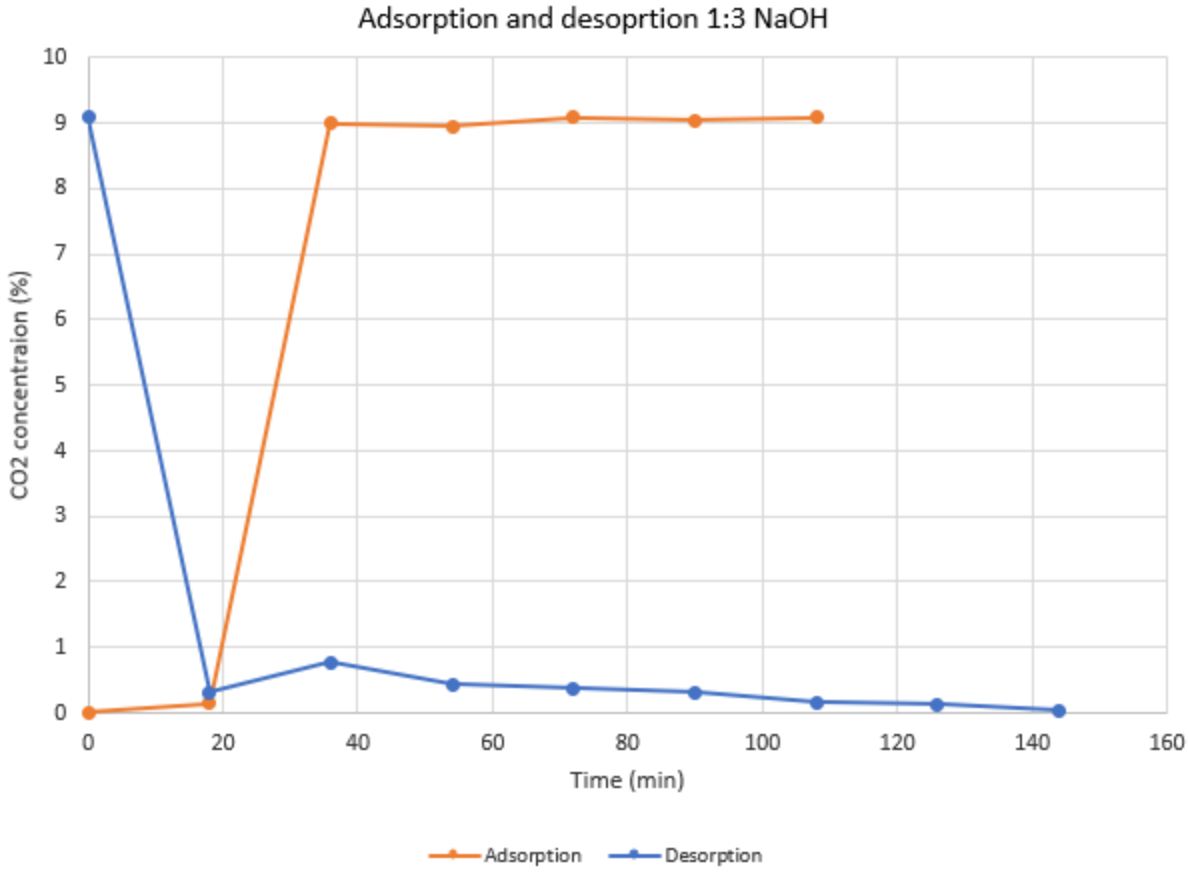

Figur 212. *CO_2 Adsorption and desorption curves for biochar derived form 1:3 NaOH ratio*

Despite the adsorption and desorption curves suggesting a relatively affective process, the calculated values in table 10 reveals that the amount of CO_2 recovered during desorption is significantly lower than the amount adsorbed. This evident from the adsorption capacity of 0,00201 mmmol/g compared to desorption capacity of only 0,0009 mmol/g.

This indicates that the regeneration of the biochar was limited, as only a small portion of the CO_2 catured was released. This behaivor may be attributed to strong interactions between CO_2 and the surface of the pores, or to it becoming trapped within the pore structure of the material.

Adsorption	0.0201 (mmol/g)
Desorption	0.0009 (mmol/g)

Table 11*. Present the adsorption-desorption for 1:3 NaOH activated biochar.*

4.6.3 Modified Biochar

For the CO_2 adsorption experiment with modified biochar, both red mud and NaOH was tested 5 times in total, but all failed. The gas flow through the colon was very slow making it impossible to achieve the wanted ratio of the mixed gas. This indicates that the gas could not flow through the biochar because of its size. However, we used the same size as on the nonmodified one and that worked. After 3 failed attempts we removed the biochar that was tested and could observe that the pressure from the gas had broken the particles into smaller sizes which was the reason for the low

flow rate. This means that the modified biochar was too fragile to run through the colon. It may be due to modified biochar containing ammonia inside the pores. This can make the particles more prone to stick and result in blockage of the colon.

4.7 Choice of methods

This section discusses the method choices made in this study and the reasoning behind them. It covers activation agent ratio choices, pyrolysis temperature choices, and separation of iron attempts.

4.7.1 Choice of ratio

The activation ratios used in this study (1:1 and 1:3) were selected based on previous activation agent research conducted within the GeViCata laboratory, where these ratios showed promising results for biomass activation. These ratios were therefore considered relevant starting points for evaluating the effect of red mud as an activation agent.

A broader range of ratios could provide a more comprehensive understanding of the relationship between activation agent loading and biochar properties. However, due to time constraints, the study was limited to these selected ratios, which were deemed sufficient to observe general trends and enable comparison with NaOH activation.

4.7.2 Separation of Iron from Biochar

The magnetic separation tests showed that both mineral particles and carbon material were attracted to the magnet. As a result, it was not possible to separate the iron while also removing a significant amount of carbon.
The unsuccessful separation can likely be explained by the fact that the iron species originating from the red mud were strongly integrated within the biochar structure during pyrolysis. This is also indicated by the SEM-EDX mapping, where we can see small particles of iron covering and being fully incorporated with the carbon.

Due to the difficulty of separating the iron from the carbon matrix without significant material losses, the biochar samples were therefore analysed and used with the red mud residues remaining in the material. Consequently, the produced material can be considered a mineral carbon rather than a pure carbon-based adsorbent.

4.7.3 Pyrolysis temperature

Knowing that a lower temperature often produces a higher yield of biochar, one could question why we didn’t change the pyrolysis temperature. Getting a big yield on your product is always a great metric; our project's focus was to promote a big specific surface area and good adsorption abilities. Higher temperatures equal more gas, which is a main factor in producing porous carbons. Therefore, we believe, through earlier work done in this lab and field, that 600 °C would be a sweet spot. At this temperature, the compromise between the biochar yield and the gas production is also more comparable with a broader research framework.

4.8 Limitations & Sources of Error

Some limitations and potential sources of experimental error should be considered when interpreting the results of this study.

It should be noted that BET measurements were performed on a single sample for each ratio. Therefore, the reported SSA should only be interpreted as indicating values rather than statistically strong averages.

Due to time limitations, only one replicate of the NaOH-activated biochar could be produced. Consequently, it was not possible to evaluate the reproducibility of the yield or assess experimental variability for this activation method.

During one of the pyrolysis runs, one ceramic boat broke, resulting in the loss of the produced biochar.

When the suspension of the activation agent and biomass was transferred from the beaker to the ceramic boat, a small extra amount of water was used to make sure all of the suspension was used, resulting in a few extra mL of water used compared to the actual ratio.

While washing the biochar after pyrolysis, filter papers were used, resulting in some small amounts of biochar being unavailable to recover. Therefore, this is a step where losses are nearly impossible to avoid.

5 Conclusion

This study investigated the production of activated biochar from acacia wood using red mud as a mineral activation agent, with NaOH-activated biochar included as a reference material. The results provide insight into how different activation agents, as well as different ratios, affect the composition, influence the structural and surface properties and impact the adsorption-desorption abilities of the material.

SEM-EDX analysis revealed that red mud activated biochar contain a significant fraction of inorganic phases, iron being the most dominant element. Increasing the red mud ratio from 1:1 to 1:3 resulted in a higher mineral content and a corresponding decrease in relative carbon content. The results also showed a heterogenous distribution of the mineral content across the surface, with localized carbon-rich areas more frequently observed in the 1:1 sample. These findings confirm that the red mud remains integrated within the carbon matrix after pyrolysis, resulting in a mineral rich carbon material rather than a purely carbon-based adsorbent.

The biochar yield showed very consistent trends for the red mud activation and pyrolysis method, where higher red mud loading resulted in higher yields due to the contribution of non-volatile mineral phases. However, after washing some variations was observed, likely due to material loss during filtration. In contrast, the NaOH-activated biochar showed an unexpected low yield. This method and result are therefore considered less reliable and is likely influenced by material loss during all of the steps of production of biochar. It should therefore not reflect a true yield.

The BET analysis demonstrated the specific surface area of each of the different biochar samples. It showed that different activation methods has a strong impact on the development of porosity. The red mud activated biochar's showed relatively low surface area ($94 m^2/g$ for 1:1 and $74 m^2/g$ for 1:3), indicating that increased mineral content may hinder a larger SSA by lower pore development or pore blockage. In contrast, the NaOH-activated biochar exhibited a significantly higher surface area ($313 m^2/g$), confirming the effectiveness of chemical activation in producing highly porous structure.

When it came to the results of the gas phase analysis from the different pyrolysis attempts all of them showed some production of greenhouse gases such as carbon monoxide. However, the red mud attempts showed higher concentrations due to their catalytical properties and higher content of Fe_2O_3. This makes the pyrolysis of red mud less favorable since it gives out greenhouse gases when the goal was to find a more environmentally friendly solution to our greenhouse gas emissions problems.

Furthermore, when analyzing the capacity of carbon dioxide adsorption and desorption between the two samples with the highest BET, we found that the biochar produced from red mud and biomass gave a slightly higher adsorption quantity. This result is particularly interesting, as it demonstrates that although the red mus activated biochar exhibited a significantly lower BET surface area compared to the NaOH activated biochar, it still showed better CO2 adsorption performance. This suggests that the adsorption behavior is not governed solely by the specific surface area. Instead, the improved performance may be related to the catatlytic or chemically active sites introduced by the mineral phases present in the red mud. However, the sodium hydroxide was better at regenerating the biochar since in the red mud the gas was more tightly bonded to components due to their catalytic sites.

In conclusion, while red mud offers a promising and more sustainable alternative as an activation agent by utilizing industrial waste, its performance remains limited compared to conventional NaOH activation. The results further indicate that the activation ratio plays a crucial role, where higher red mud loading increases mineral content but negatively affects pore development and surface area. However may contribute to higher adsorption performances. Future improvements in optimizing the activation ratio, enhancing pore structure, and reducing unwanted gas formation are necessary for red mud–based biochar to become a competitive option for CO_2 capture applications.

6 Future work

For future work in the same field, different attempts to separate out the red mud residues should be considered. For example, experiments of removing the red mud before pyrolysis or finding other ways to allow easier separation of biochar and red mud could be interesting.

More sensitive techniques and analysis methods such as XPS could be used to get more detailed information about the impregnation of ammonia into the biochar.

As well as other ways of integrating and optimizing the modification with ammonia by changing time, temperature etc.

References

[1] Legg, S. IPCC, 2021: Climate Change 2021—The Physical Science Basis. Interaction 2021, 49 (4), 44–45.

[2] Sevilla, M.; Díez, N.; Fuertes, A. B. More Sustainable Chemical Activation Strategies for the Production of Porous Carbons. ChemSusChem 2021, 14 (1), 94–117. https://doi.org/10.1002/cssc.202001838.

[3] Ma, Z.; Yang, Y.; Wu, Y.; Xu, J.; Peng, H.; Liu, X.; Zhang, W.; Wang, S. In-Depth Comparison of the Physicochemical Characteristics of Bio-Char Derived from Biomass Pseudo Components: Hemicellulose, Cellulose, and Lignin. Journal of Analytical and Applied Pyrolysis 2019, 140, 195–204. https://doi.org/10.1016/j.jaap.2019.03.015.

[4] Lillo-Ródenas, M. A.; Lozano-Castelló, D.; Cazorla-Amorós, D.; Linares-Solano, A. Preparation of Activated Carbons from Spanish Anthracite: II. Activation by NaOH. Carbon 2001, 39 (5), 751–759. https://doi.org/10.1016/S0008-6223(00)00186-X.

[5] Sevilla, M.; Mokaya, R. Energy Storage Applications of Activated Carbons: Supercapacitors and Hydrogen Storage. Energy Environ. Sci. 2014, 7 (4), 1250–1280. https://doi.org/10.1039/C3EE43525C.

[6] Sushil, S.; Batra, V. S. Catalytic Applications of Red Mud, an Aluminium Industry Waste: A Review. Applied Catalysis B: Environmental 2008, 81 (1), 64–77. https://doi.org/10.1016/j.apcatb.2007.12.002.

[7] Shafeeyan, M. S.; Daud, W. M. A. W.; Houshmand, A.; Shamiri, A. A Review on Surface Modification of Activated Carbon for Carbon Dioxide Adsorption. Journal of Analytical and Applied Pyrolysis 2010, 89 (2), 143–151. https://doi.org/10.1016/j.jaap.2010.07.006.

[8] Lignocellulosic Biomass - an overview | ScienceDirect Topics. https://www.sciencedirect.com/topics/engineering/lignocellulosic-biomass (accessed 2026-03-23).

[9] Waters, C. L.; Janupala, R. R.; Mallinson, R. G.; Lobban, L. L. Staged Thermal Fractionation for Segregation of Lignin and Cellulose Pyrolysis Products: An Experimental Study of Residence Time and Temperature Effects. Journal of Analytical and Applied Pyrolysis 2017, 126, 380–389. https://doi.org/10.1016/j.jaap.2017.05.008.

[10] Kopp Alves, A.; Hauschild, T.; Basegio, T. M.; Amorim Berutti, F. Influence of Lignin and Cellulose from Termite-Processed Biomass on Biochar Production and Evaluation of Chromium VI Adsorption. Sci Rep 2024, 14 (1), 14937. https://doi.org/10.1038/s41598-024-65959-5.

[11] Rahman, F.; Md Salim, R.; Mohktar, J. Optimizing Wood Pellet Quality: Physical Properties of Acacia Hybrid and Pine Wood Waste for Industrial Applications. Journal of Renewable Materials 2026, 14 (2). https://doi.org/10.32604/jrm.2026.02025-0066.

[12] Oginni, O.; Singh, K.; Oporto, G.; Dawson-Andoh, B.; McDonald, L.; Sabolsky, E. Influence of One-Step and Two-Step KOH Activation on Activated Carbon Characteristics. Bioresource Technology Reports 2019, 7, 100266. https://doi.org/10.1016/j.biteb.2019.100266.

[13] Mohammed, J.; Nasri, N. S.; Zaini, M. A. A.; Dadum, U. H.; Ahmed, M. M. Comparison on the Characteristics of Bio-Based Porous Carbons by Physical and Novel Chemical Activation. Applied Mechanics and Materials 2014, 554, 22–26. https://doi.org/10.4028/www.scientific.net/AMM.554.22.

[14] Manocha, S. M. Porous Carbons. Sadhana 2003, 28 (1), 335–348. https://doi.org/10.1007/BF02717142.

[15] Guo, F.; Peng, K.; Liang, S.; Jia, X.; Jiang, X.; Qian, L. One-Step Synthesis of Biomass Activated Char Supported Copper Nanoparticles for Catalytic Cracking of Biomass Primary Tar. Energy 2019, 180, 584–593. https://doi.org/10.1016/j.energy.2019.05.115.

[16] Hoang, T.-D.; Liu, Y.; Le, M. T. Synthesis and Characterization of Biochars and Activated Carbons Derived from Various Biomasses. Sustainability 2024, 16 (13), 5495. https://doi.org/10.3390/su16135495.

[17] Danish, M.; Hashim, R.; Ibrahim, M. N. M.; Sulaiman, O. Effect of Acidic Activating Agents on Surface Area and Surface Functional Groups of Activated Carbons Produced from Acacia Mangium Wood. Journal of Analytical and Applied Pyrolysis 2013, 104, 418–425. https://doi.org/10.1016/j.jaap.2013.06.003.

[18] Zhou, X.; Zhang, L.; Chen, Q.; Xiao, X.; Wang, T.; Cheng, S.; Li, J. Study on the Mechanism and Reaction Characteristics of Red-Mud-Catalyzed Pyrolysis of Corn Stover. Fuel 2023, 338, 127290. https://doi.org/10.1016/j.fuel.2022.127290.

[19] Huang, Z.; He, F.; Zheng, A.; Zhao, K.; Chang, S.; Zhao, Z.; Li, H. Synthesis Gas Production from Biomass Gasification Using Steam Coupling with Natural Hematite as Oxygen Carrier. Energy 2013, 53, 244–251. https://doi.org/10.1016/j.energy.2013.02.068.

[20] Dhila, H.; Bhapkar, A.; Bhame, S. Metal Oxide/Biochar Hybrid Nanocomposites for Adsorption and Photocatalytic Degradation of Textile Dye Effluents: A Review. Desalination and Water Treatment 2025, 321, 101004. https://doi.org/10.1016/j.dwt.2025.101004.

[21] Silveira, N. C. G.; Martins, M. L. F.; Bezerra, A. C. S.; Araújo, F. G. S. Red Mud from the Aluminium Industry: Production, Characteristics, and Alternative Applications in Construction Materials—A Review. Sustainability 2021, 13 (22), 12741. https://doi.org/10.3390/su132212741.

[22] Yang, Y.; Xiao, P.; Wen, M.; Liu, T.; Yang, J.; Dai, S.; Zhao, Y.; Huang, Q.; Liu, Z.; Li, B. A Review on the Modified Red Mud for Biomass Catalytic Pyrolysis: Preparation, Mechanisms and Perspectives. Journal of Analytical and Applied Pyrolysis 2024, 178, 106430. https://doi.org/10.1016/j.jaap.2024.106430.

[23] Lillo-Ródenas, M. A.; Cazorla-Amorós, D.; Linares-Solano, A. Understanding Chemical Reactions between Carbons and NaOH and KOH: An Insight into the Chemical Activation Mechanism. Carbon 2003, 41 (2), 267–275. https://doi.org/10.1016/S0008-6223(02)00279-8.

[24] Bùi Thị Thu Huệ. *Nghiên cứu tổng hợp và biến tính than hoạt tính từ tre phế thải, ứng dụng hấp phụ CO_2*. Đồ án tốt nghiệp, Đại học Bách Khoa Hà Nội, 2024.

[25] Lehmann, J.; Joseph, S. Biochar for Environmental Management: Science and Technology; Earthscan: London, 2009.

[26] Yang, H.; Yan, R.; Chen, H.; Lee, D. H.; Zheng, C. Characteristics of Hemicellulose, Cellulose and Lignin Pyrolysis. Fuel 2007, 86 (12), 1781–1788. https://doi.org/10.1016/j.fuel.2006.12.013.

[27] Li, D.-C.; Jiang, H. The Thermochemical Conversion of Non-Lignocellulosic Biomass to Form Biochar: A Review on Characterizations and Mechanism Elucidation. Bioresource Technology 2017, 246, 57–68. https://doi.org/10.1016/j.biortech.2017.07.029.

[28] González, J. F.; Román, S.; Encinar, J. M.; Martínez, G. Pyrolysis of Various Biomass Residues and Char Utilization for the Production of Activated Carbons. Journal of Analytical and Applied Pyrolysis 2009, 85 (1), 134–141. https://doi.org/10.1016/j.jaap.2008.11.035.

[29] González, J. F.; Ramiro, A.; González-García, C. M.; Gañán, J.; Encinar, J. M.; Sabio, E.; Rubiales, J. Pyrolysis of Almond Shells. Energy Applications of Fractions. Ind. Eng. Chem. Res. 2005, 44 (9), 3003–3012. https://doi.org/10.1021/ie0490942.

[30] Kumar Mishra, R.; Singh, B.; Acharya, B. A Comprehensive Review on Activated Carbon from Pyrolysis of Lignocellulosic Biomass: An Application for Energy and the Environment. Carbon Resources Conversion 2024, 7 (4), 100228. https://doi.org/10.1016/j.crcon.2024.100228.

[31] Fazzalari, A.; Abou-Zaid, M.; Briens, C.; Briens, L. Impact of Post-pyrolysis Wash on Biochar Properties. Can J Chem Eng 2023, 101 (2), 782–796. https://doi.org/10.1002/cjce.24426.

[32] Huang, X.; Tie, Y.; Jiang, J.; Deng, L.; Che, D. Water Washing of Biomass and Biochar. Sustainable Energy Technologies and Assessments 2023, 56, 103066. https://doi.org/10.1016/j.seta.2023.103066.

[33] Lee, J.-E.; Jayakody, J.; Kim, J.-I.; Jeong, J.-W.; Choi, K.-M.; Kim, T.-S.; Seo, C.; Azimi, I.; Hyun, J.; Ryu, B. The Influence of Solvent Choice on the Extraction of Bioactive Compounds from

Asteraceae: A Comparative Review. Foods 2024, 13 (19), 3151. https://doi.org/10.3390/foods13193151.

[34] Plaza, M. G.; Pevida, C.; Arias, B.; Fermoso, J.; Arenillas, A.; Rubiera, F.; Pis, J. J. Application of Thermogravimetric Analysis to the Evaluation of Aminated Solid Sorbents for CO_2 Capture. J Therm Anal Calorim 2008, 92 (2), 601–606. https://doi.org/10.1007/s10973-007-8493-x.

[35] Plaza, M. G.; Pevida, C.; Arenillas, A.; Rubiera, F.; Pis, J. J. CO_2 Capture by Adsorption with Nitrogen Enriched Carbons. Fuel 2007, 86 (14), 2204–2212. https://doi.org/10.1016/j.fuel.2007.06.001.

[36] Stoeckli, F.; Centeno, T. A.; Fuertes, A. B.; Muñiz, J. Porous Structure of Polyarylamide-Based Activated Carbon Fibres. Carbon 1996, 34 (10), 1201–1206. https://doi.org/10.1016/0008-6223(96)00088-7.

[37] Zhang, H.; Jiang, F.; Zhang, X.; Hu, S.; Li, J.; Zhang, H.; Liu, K. CO_2 Adsorption Performance of Nitrogen-Doped Activated Carbon from Banana Pseudo-Stem by Urea-Assisted High-Pressure CO_2-Hydrothermal Treatment. Separation and Purification Technology 2025, 366, 132773. https://doi.org/10.1016/j.seppur.2025.132773.

[38] Skubiszewska-Zięba, J.; Sydorchuk, V. V.; Gun'ko, V. M.; Leboda, R. Hydrothermal Modification of Carbon Adsorbents. Adsorption 2011, 17 (6), 919–927. https://doi.org/10.1007/s10450-011-9369-8.

[39] He, L.; Wang, Y.; Gao, H.; Liu, Z.; Xie, Z. Nitrogen Doped Carbon for Pd-Catalyzed Hydropurification of Crude Terephthalic Acid: Roles of Nitrogen Species. RSC Advances 2021, 11 (53), 33646–33652. https://doi.org/10.1039/D1RA06479G.

[40] Shafeeyan, M. S.; Daud, W. M. A. W.; Houshmand, A.; Arami-Niya, A. Ammonia Modification of Activated Carbon to Enhance Carbon Dioxide Adsorption: Effect of Pre-Oxidation. Applied Surface Science 2011, 257 (9), 3936–3942. https://doi.org/10.1016/j.apsusc.2010.11.127.

[41] Luo, L.; Chen, T.; Zhao, W.; Fan, M. Hydrothermal Doping of Nitrogen in Bamboo-Based Super Activated Carbon for Hydrogen Storage. BioResources 2017, 12 (3), 6237–6250.

[42] Fan, X.; Yu, C.; Yang, J.; Ling, Z.; Qiu, J. Hydrothermal Synthesis and Activation of Graphene-Incorporated Nitrogen-Rich Carbon Composite for High-Performance Supercapacitors. Carbon 2014, 70, 130–141. https://doi.org/10.1016/j.carbon.2013.12.081.

[43] Kundu, S.; Khandaker, T.; Mia Anik, M. A.-A.; Kamrul Hasan, M.; Kumar Dhar, P.; Kumar Dutta, S.; Abdul Latif, M.; Sarwar Hossain, M. A Comprehensive Review of Enhanced CO 2 Capture Using Activated Carbon Derived from Biomass Feedstock. RSC Advances 2024, 14 (40), 29693–29736. https://doi.org/10.1039/D4RA04537H.

[44] Gunawardene, O. H. P.; Gunathilake, C. A.; Vikrant, K.; Amaraweera, S. M. Carbon Dioxide Capture through Physical and Chemical Adsorption Using Porous Carbon Materials: A Review. Atmosphere 2022, 13 (3), 397. https://doi.org/10.3390/atmos13030397.

[45] Serafin, J.; Dziejarski, B. Activated Carbons—Preparation, Characterization and Their Application in CO_2 Capture: A Review. Environ Sci Pollut Res 2024, 31 (28), 40008–40062. https://doi.org/10.1007/s11356-023-28023-9.

[46] Kennedy, D. A.; Tezel, F. H. Cation Exchange Modification of Clinoptilolite – Screening Analysis for Potential Equilibrium and Kinetic Adsorption Separations Involving Methane, Nitrogen, and Carbon Dioxide. Microporous and Mesoporous Materials 2018, 262, 235–250. https://doi.org/10.1016/j.micromeso.2017.11.054.

[47] Díaz, E.; Ordóñez, S.; Vega, A.; Coca, J. Adsorption Characterisation of Different Volatile Organic Compounds over Alumina, Zeolites and Activated Carbon Using Inverse Gas Chromatography. Journal of Chromatography A 2004, 1049 (1), 139–146. https://doi.org/10.1016/j.chroma.2004.07.061.

[48] Goldstein, J.; Newbury, D. E.; Michael, J. R.; Ritchie, N. W. M.; Scott, J. H. J.; Joy, D. C. Scanning Electron Microscopy and X-Ray Microanalysis, Fourth edition.; Springer: New York, NY, U.S.A, 2018.

[49] Advanced Applications of Biobased Materials: Food, Biomedical, and Environmental Applications; Ahmed, S., Tomer, A., Eds.; Elsevier: Amsterdam, 2023.

[50] The IUPAC Compendium of Chemical Terminology: The Gold Book, 5th ed.; Gold, V., McNaught, A., The International Union of Pure and Applied Chemistry (IUPAC), Eds.; International Union of Pure and Applied Chemistry (IUPAC): Research Triangle Park, NC, 2025. https://doi.org/10.1351/goldbook.
0)
[51] BET Theory | Anton Paar Wiki. Anton Paar. https://wiki.anton-paar.com/en/bet-theory/ (accessed 2026-03-23).

Attachments

Attachment 1: Shows different gasses detected during the pyrolysis process of the 1.1 red mud sample.

1.1 Redmud

Replicates	Temperature range the gas was captured in	Area			
		H2		CH4	CO
1	400-500	0	43,717	0,001	0
2		0	45,457	0,013	0,039
3		0	46,68	0,004	0,021
	Average	0,000000	45,28466667	0,006000	0,02
concentration		0	0,376238923	0,000117925	0,000286627
1	500-550	0	45,447	0,042	0,473
2		0	45,225	0,023	0,558
3		0	45,328	0,054	0,421
	Average	0	45,33333333	0,039666667	0,484
concentration		0	0,376643261	0,000779617	0,006936383
1	550+	0	46,356	0,088	0,096
2		0	45,47	0,057	0,102
3		0	46,049	0,154	0,148
	Average	0	45,95833333	0,099666667	0,115333333
concentration		0	0,381835953	0,001958868	0,001652885

1.3 Redmud

Replicates	Temperature range the gas was captured in	Area			
		H2	N2	CH4	CO
1	400-500	0	46,097	0,003	0,007
2		0	46,174	0,005	0,02
3		-	-	-	-
	Average	0,000000	46,135500	0,004000	0,013500
concentration		0	0,383307908	7,86168E-05	0,000193473
1	500-550	0	47,158	0,01	0,184
2		0	45,805	0,015	0,18
3		-	-	-	-
	Average	0	46,4815	0,0125	0,182
concentration		0	0,386182582	0,000245677	0,002608309
1	550+	0	43,307	0,357	1,022
2		0	45,112	0,124	0,69
3		-	-	-	-
	Average	0	44,2095	0,2405	0,856
concentration		0	0,367306108	0,004726835	0,012267653

1.3 NaOH

Replicates	Temperature range the gas was captured in	Area			
		H2	N2	CH4	CO
1	400-500	0	46,2918	0,0045	0,0016
	Average	0,000000	46,2918	0,0045	0,0016
concentration		0	0,384606496	8,84439E-05	2,29302E-05
1	500-550	0	411,2396	0,1173	0,0031
	Average	0	411,2396	0,1173	0,0031
concentration		0	3,41670494	0,002305437	4,44272E-05
1	550+	0	38,71	0,6665	0,0284
	Average		38,71	0,6665	0,0284
concentration		0	0,321614573	0,013099523	0,000407011

Tabell:

1.1 Redmud

Mass of the biochar: 0.192 (g)		Adsorption-Desorption						Bypass	
		time (min)	Peak Area		CO2 Concentration			Time (min)	S(peak) CO2
			N2	CO2	%CO2	ppm	S (ppm.min)	18	15,3592
Adsorption 25oC, 1bar		0		0	0	0,0000	277,6632	36	15,4640
Desorption 150oC, 1bar		18		0	0	0,0000	201,7703	54	15,454
Ratio: 10% CO2 - 90% N2		36		11,8339	7,671531553	8,4325	112,7040		
Total flow rate: 94 mL/min		54		13,8880	9,003137614	9,8962	94,3893	average	15,4257
CO2 standard peak	15,4257	72		14,6897	9,522853587	10,4675	85,7879	Actual CO2% in the flow	10,0000
CO2 percentage concentraion	10,9920	90		15,2292	9,872593848	10,8520	80,8812		
		108		15,4548	10,01884297	11,0127	78,7584		
		126		15,5602	10,08717036	11,0878	78,2608		
		144		15,5324	10,06914852	11,0680	172,5384		
		162		0,8596	0,557250655	0,6125	8,2159		
		180		0,4215	0,273244708	0,3004	5,6513		
		198		0,4597	0,298008523	0,3276	4,8759	Bắt đầu quá trình nhả hấp phụ	
		216		0,3006	0,19486918	0,2142	4,5187		
		234		0,404	0,261900029	0,2879	2,7525		
		252		0,0252	0,016336338	0,0180	0,1616		
		270		0	0,0000	0,0000	0,0000		
					Calculation for adsorption	11,0878	1182,7534		
					Calculation for desoprtion	1,7605	26,1760		
					Adsorption		0,0259	mmol/g	
					Desorption		0,0006	mmol/g	

NaOH

Mass of the biochar: 0.198 (g)		Adsorption-Desorption						Bypass	
		time (min)	Peak Area		CO2 Concentration			Time (min)	S(peak) CO2
			N2	CO2	%CO2	ppm	S (ppm.min)	18	15,0668
Adsorption 25oC, 1bar		0		0	0	0,0000	276,2247	36	15,7370
Desorption 150oC, 1bar		18		0,2243	0,145084088	0,1598	187,2162	54	15,4895
Ratio: 10% CO2 - 90% N2		36		13,8790	8,997303208	9,8898	100,1894		
Total flow rate: 85,2 mL/min		54		13,7943	8,942394959	9,8295	99,3467	average	15,4311
CO2 standard peak	15,4311	72		14,0104	9,082485544	9,9835	98,4161	Actual CO2% in the flow	10,0000
CO2 percentage concentraion	10%	90		13,9394	9,036458558	9,9329	98,4084		
		108		14,0116	9,083263465	9,9843	184,7247		
		126		0,4802	0,311298004	0,3422	10,7030		
		144		1,1887	0,770595455	0,8470	11,8939		
		162		0,6659	0,43168126	0,4745	7,9357		
		180		0,5715	0,370484818	0,4072	6,7146		
		198		0,4755	0,308251147	0,3388	4,5886	Bắt đầu quá trình nhả hấp phụ	
		216		0,24	0,155584175	0,1710	2,8455		
		234		0,2037	0,132052069	0,1452	1,5873		
		252		0,0438	0,028394112	0,0312	0,2809		
		270			0,0000	0,0000	0,0000		
					Calculation for adsorption	49,7798	1044,5261		
					Calculation for desoprtion	2,7572	46,5494		
					Adsorption		0,0201	mmol/g	
					Desorption		0,0009	mmol/g	

Tabel 1: Yields of the produced biochar.

Department of Chemistry and Chemical Engineering
CHALMERS UNIVERSITY OF TECHNOLOGY
Göteborg, Sweden 2026
www.chalmers.se

CHALMERS